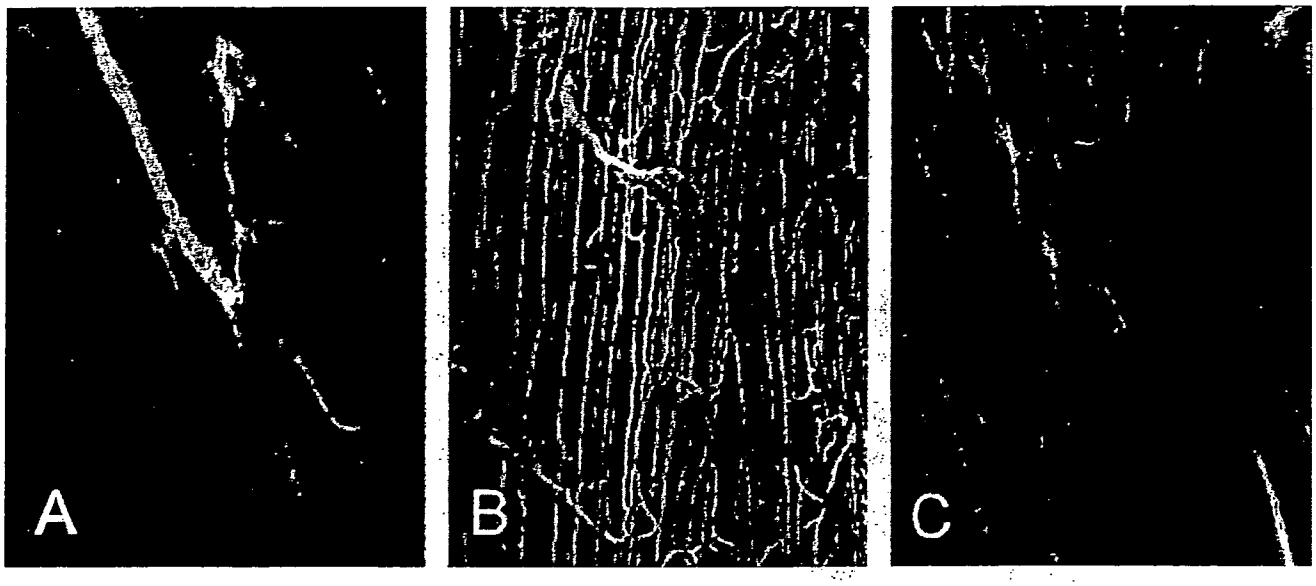

Fig. 6. FITC angiography. FITC angiograms were evaluated on day 14. A: in an animal of the Wild group; B: in an animal of the iNOS-KO group; C: in an animal of the Wild + AG group. Clear angiogenesis was visualized in the iNOS-KO group compared with the control group and aminoguanidine-treated group.

References

[1] Rosamond, W.D., Chambless, L.E., Folsom, A.R., Cooper, L.S., Conwill, D.E., Clegg, L., Wang, C.H., and Heiss, G.: Trends in the incidence of myocardial infarction and in mortality due to coronary heart disease, 1987 to 1994. *N. Engl. J. Med.*, **339**, 861-867, 1998.

[2] Mukherjee, D., Bhatt, D.L., Roe, M.T., Patel, V., and Ellis, S.G.: Direct myocardial revascularization and angiogenesis-How many patients might be eligible? *Am. J. Cardiology.*, **84**, 598-600, 1999.

[3] Isner, J.M. and Asahara, T.: Angiogenesis and vasculogenesis as therapeutic strategies for postnatal neovascularization. *J. Clin. Invest.*, **103**, 1231-1236, 1999.

[4] Carmeliet, P., Ng, Y.S., Nuyens, D., Theilmeier, G., Brusselmans, K., Cornelissen, I., Ehler, E., Kakkar, V.V., Stalmans, I., Mattot, V., Perriard, J.C., Dewerchin, M., Flameng, W., Nagy, A., Lupu, F., Moons, L., Collen, D., Amore, P.A.D., and Shima, D.T.: Impaired myocardial angiogenesis and ischemic cardiomyopathy in mice lacking the vascular endothelial growth factor isoforms $VEGF_{164}$ and $VEGF_{188}$. *Nature. Med.*, **5**, 495-502, 1999.

[5] Jayasnkar V., Woo J., Bish L.T., Pirolli T.J., Chatterjee S., Berry M.F., Burdick J., Gardner T.J., and Sweeney H.L.: Gene transfer of hepatocyte growth factor attenuates postinfarction heart failure. *Circulation*, **108**[suppl II], II-230-II-236, 2003.

[6] Taniyama, Y., Morishita, R., Hiraoka, K., Aoki, M., Nakagami, H., Yamasaki, K., Matsumoto, K., Nakamura, T., Kaneda, Y., and Ogihara,T.: Therapeutic angiogenesis induced by human hepatocyte growth factor gene in rat diabetic hind limb ischemia model. Molecular mechanisms of delayed angiogenesis in diabetes. *Circulation*, **104**, 2344-2350, 2001.

[7] Grines, C.L., Watkins, M.W., Helmer, G., Penny, W., Brinker, J., Marmur, J.D., West, A., Rade, J.J., Marrott, P., Hammond, H.K. and Engler, R.L.: Angiogenic gene therapy (AGENT) trial in patients with stable angina pectoris. *Circulation*, **105**, 1291-1297, 2002.

[8] Tateishi-Yuyama, E., Matsubara, H., Murohara, T., Ikeda, U., Shintani, S., Masaki, H., Amano, K., Kishimoto, Y., Yoshimoto, K., Akashi, H., Shimada, K., Iwasaka, T., and Imaizumi, T.: Therapeutic angiogenesis for patients with limb ischemia by autologous transplantation of bone-marrow cells: a pilot study and a randomized controlled trial. *Lancet*, **360**, 427-435, 2002.

[9] Randomski, M.W., Vallance, P., Whitley, G., Foxwell, N., and Moncada, S.: Platelet adhesion to human vascular endothelium is modulated by constitutive and cytokine induced nitric oxide. *Cardiovasc. Res.*, **27**, 1380-1382, 1993.

[10] Förstermann, U., Closs, E.I., Pollock, J.S., Nakane, M., Schwarz, P., Gath, I., and Kleinert, H.: Nitric oxide synthase isozymes characterization, molecular cloning, and functions. *Hypertension*, **23**, 1121-1131, 1994.

[11] Ziche, M., Morbidelli, L., Masini, E., Amerini, S., Granger, H.J., Maggi, C.A., Geppetti, P., and Ledda, F.: Nitric Oxide Mediates Angiogenesis *in vivo* and endothelial cell growth and migration *in vitro* promoted by substance P. *J. Clin. Invest.*, **94**, 2036-2044, 1994.

[12] Papapetropoulos, A., Desai, K.M., Rudic, R.D., Mayer, B., Zhang, R., Ruiz-Torres, M.P., García-Cardeña, G., Madri, J.A., and Sessa, W.C.: Nitric oxide synthase inhibitors attenuate transforming-growth-factor-β_1-stimulated capillary organization *in vitro*. *Am. J. pathol.*, **150**, 1835-1844, 1997.

[13] Ziche, M., Morbidelli, L., Choudhuri, R., Zhang, H.T., Donnini, S., Granger, H.J., and Bicknell, R.: Nitric oxide

synthase lies downstream from vascular endothelial growth factor-induced but not basic fibroblast growth factor-induced angiogenesis. *J. Clin. Invest.*, **99**, 2625-2634, 1997.

[14] Papapetropoulos, A., García-Cardeña, G., Madri, J.A., and Sessa, W.C.: Nitric oxide production contributes to the angiogenic properties of vascular endothelial growth factor in human endothelial cells. *J. Clin. Invest.*, **100**, 3131-3139, 1997.

[15] Park, K.M., Byun, J.Y., Kramers, C., Kim, J.I., Huang, P.L., and Bonventre, J.V.: Inducible nitoric-oxide synthase is an important contributor to prolonged protective effects of ischemic preconditioning in the mouse kidney. *J. Biol. Chem.*, **278**, 27256-27266, 2003.

[16] Murohara, T., Asahara, T., Silver, M., Bauters, C., Masuda, H., Kalka, C., Kearney, M., Chen, D., Symes, J.F., Fishman, M.C., Huang, P.L., and Isner, J.M.: Nitric oxide synthase modulates angiogenesis in response to tissue ischemia. *J. Clin. Invest.*, **101**, 2567-2578, 1998.

[17] Brevetti, L.S., Chang, D.S., Tang, G.L., Sarkar, R., and Messina, L.M.: Overexpression of endothelial nitric oxide synthase increases skeletal muscle blood flow and oxygenation in severe rat hind limb ischemia. *J. Vasc. Surg.*, **38**, 820-826, 2003.

[18] Wildhirt, S.M., Suzuki, H., Horstman, D., Weismüller, S., Dudek, R.R., Akiyama, K., and Reichart, B.: Selective modulation of inducible nitric oxide synthase isozyme in myocardial infarction. *Circulation*, **96**, 1616-1623, 1997.

[19] Misko, T.P., Moore, W.M., Kasten, T.P., Nickols, G.A., Corbett, J.A., Tilton, R.G., McDaniel, M.L., Williamson, J.R., and Currie, M.G.: Selective inhibition of the inducible nitric oxide synthase by aminoguanidine. *Eur. J. Pharmacol.*, **233**, 119-125, 1993.

[20] Joly, G.A., Ayres, M., Chelly, F., and Kilboum, R.G.: Effects of NG-methyl-L-arginine, NG-nitro-L-arginine, and aminoguanidine on constitutive and inducible nitric oxide synthase in rat aorta. *Biochem. Biophys. Res. Commun.*, **199**, 147-154, 1994.

[21] Cross, A.H., Misko T.P., Lin, R.F., Hickey, W.F., Trotter, J.L., and Tilton, R.G.: Aminoguanidine, an inhibitor of inducible nitric oxide synthase, ameliorates experimental autoimmune encephalomyelitis in SJL mice. *J. Clin. Invest.*, **93**, 2684-2690, 1994.

[22] Niu, X.L., Yang, X., Hoshiai, K., Tanaka, K., Swamura, S., Koga, Y., and Nakazawa, H.: Inducible nitric oxide synthase deficiency dose not affect the susceptibility of mice to atherosclerosis but increases collagen content in lesions. *Circulation*, **103**, 1115-1120, 2001.

[23] Wolff, D.J., Gauld, D.S., Neulander, M.J., and Southan, G.: Inactivation of nitric oxide synthase by substituted aminoguanidines and aminoisothioureas. *J. Pharmacol. Exp. Ther.*, **283**, 265-273, 1997.

[24] Wildhirt, S.M., Schulze, C., Conrad, N., Kornberg, A., Horstman, D., and Reichart, B.: Aminoguanidine inhibits inducible NOS and reverses cardiac dysfunction late after ischemia and reperfusion-implications for iNOS-mediated myocardial stunning. *Thorac. Cardiovasc. Surg.*, **47**, 137-143, 1999.

[25] Tamarat, R., Silvestre, J.S., Huijberts, M., Benessiano, J., Ebrahimian, T.G., Duriez, M., Wautier, M.P., Wautier, J.L., and Lévy, B.I.: Blockade of advanced glycation end-product formation restores ischemia-induced angiogenesis in diabetic mice. *Proc. Natl. Acad. Sci. U. S. A.*, **100**, 8555-8560, 2003.

[26] Couffinhal, T., Silver, M., Zheng, L.P., Kearney, M., Witzenbichler, B., and Isner, J.M.: Mouse model of angiogenesis. *Am. J. Pathol.*, **152**, 1667-1679, 1998.

[27] Kasahara, H., Tanaka, E., Fukuyama, N., Sato, E., Sakamoto, H., Tabata, Y., Ando, K., Iseki, H., Shinozaki, Y., Kimura, K., Kuwabara, E., Koide, S., Nakazawa, H., and Mori, H.: Biodegradable gelatin hydrogel potentiates the angiogenic effect of fibroblast growth factor 4 plasmid in rabbit hindlimb ischemia. *J. Am. Coll. Cardiol.*, **41**, 1056-1062, 2003.

[28] Tanaka, E., Hattan, N., Ando, K., Ueno, H., Sugio, Y., Mohammed, M.U., Voltchikhina, S.A., and Mori H.: Amelioration of microvascular myocardial ischemia by gene transfer of vascular endothelial growth factor in rabbits. *J. Thorac. Cardiovasc. Surg.*, **120**, 720-728, 2000.

[29] Lindén, M., Sirsjö, A., Lindbom, L., Nilsson, G., and Gidlöf, A.: Laser-Doppler perfusion imaging of microvascular blood flow in rabbit tenuissimus muscle. *Am. J. Physiol. Heart Circ. Physiol.*, **269**, H1496-H1500, 1995.

[30] Kuwabara, E., Furuyama, F., Ito, K., Tanaka, E., Hattan, N., Fujikura, H., Kimura, K., Goto, T., Hayashi, T., Taira, H., Shinozaki, Y., Umetani, K., Hyodo, K., Tanioka, K., Mochizuki, R., Kawai, T., Koide, S., and Mori, H.: Inhomogeneous vasodilatory responses of rat tail arteries to heat stress: evaluation by synchrotron radiation microangiography. *Jpn. J. Physiol.*, **52**, 403-408, 2002.

[31] Sekka, T., Volchikhina, S.A., Tanaka, A., Hasegawa, M., Tanaka, Y., Ohtani, Y., Tajima, T., Makuuchi, H., Tanaka, E., Iwata, Y., Sato, S., Hyodo, K., Ando, M., Umetani, K., Kubota, M., Tanioka, K., and Mori, H.: Visualization, quantification and therapeutic evaluation of angiogenic vessels in cancer by synchrotron microangiography. *J. Synchrotron Rad.*, **7**, 361-367, 2000.

[32] Takeshita, S., Zheng, L.P., Brogi, E., Kearney, M., Pu, L.G., Bunting, S., Ferrara, N., Symes, J.F., and Isner, J.M.: Therapeutic angiogenesis: a single intra-arterial bolus of vascular endothelial growth factor augments revascularization in a rabbit ischemic hind limb model. *J. Clin. Invest.*, **93**, 662-670, 1994.

[33] Takeshita, S., Isshiki, T., Ochiai, M., Eto, K., Mori, H., Tanaka, E., Umetani, K. and Sato, T.: Endothelium-dependent relaxation of collateral microvessels after intramuscular gene transfer of vascular endothelial growth factor in a rat model of hindlimb ischemia. *Circulation*, **98**, 1261-1263, 1998.

[34] Chung, N.A.Y., Lydakis, C., Belgore, F., Blann, A.D., and Lip, G.Y.H.: Angiogenesis in myocardial infarction An acute or chronic process? *Eur. Heart J.*, **23**, 1604-1608, 2002.

[35] Gavin, J.B., Maxwell, L., and Edgar, S.G.: Microvascular Involvement in Cardiac Pathology. *J. Mol. Cell. Cardiol.*, **30**, 2531-2540, 1998.

[36] Sennlaub, F., Courtois, Y., and Goureau, O. Inducible nitric

oxide synthase mediates the change from retinal to vitreal neovascularization in ischemic retinopathy. *J. Clin. Invest.*, **107**, 717-725 2001.

[37] Itoh, J., Kawai, K., Serizawa, A., Yasumura, K., Ogawa, K., and Osamura, R.Y.: A new approach to three-dimensional reconstructed imaging of hormone-secreting cells and their microvessel environments in rat pituitary glands by confocal laser scanning microscopy. *J. Histochem. Cytochem.*, **48**, 569-577, 2000.

[38] Itoh, J., Yasumasa, K., Takeshita, T., Ishikawa, H., Kobayashi, H., Ogawa, K., Kawai, K., Serizawa, A., and Osamura, R.Y.: Three-dimensional imaging of tumor angiogenesis. *Analyt. Quant. Cytol. Histol.*, **22**, 85-90, 2000.

[39] Kobzik, L., Reid, M.B., Bredt, D.S., and Stamler, J.S.: Nitric oxide in skeletal muscle. *Nature*, **372**, 546-548 1994.

[40] Brenman, J.E., Christopherson, K.S., Craven, S.E., McGee, A.W., and Bredt, D.S.: Cloning and Characterization of Postsynaptic Density 93, a Nitric Oxide Synthase Interacting Protein. *J. Neurosci.*, **16**, 7407-7415, 1996.

[41] Dreyer, J., Schleicher, M., Tappe, A., Schilling, K., Kuner, T., Kusumawidijaja, G., Müller-Esterl, W., Oess, S., and Kuner, R.: Nitric Oxide Synthase (NOS)-Interacting Protein Interacts with Neuronal NOS and Regulates Its Distribution and Activity. *J. Neurosci.*, **24**, 10454-10465, 2004.

[42] Sharshar, T., Gray, F., Geoffroy, L.G., Hopkinson, N.S., Ross, E., Dorandeu, A., Orlikowski, D., Raphael, J.C., Gajdos, P., and Annane, D.: Apoptosis of neurons in cardiovascular autonomic centres triggered by inducible nitric oxide synthase after death from septic shock. *Lancet*, **362**, 1799-1805 2003.

[43] Liang, F., Gao, E., Tao, L., Liu, H., Ou, Y., Christopher, T.A., Lopez, B.L., and Ma, X.L.: Critical timing of L-arginine treatment in post-ischemic myocardial apoptosis—role of NOS isoforms. *Cardiovasc. Res.*, **62**, 568-577, 2004.

[44] Kane, A.J., Barker, J.E., Mitchell, G.M., Theile, D.R.B., Romero, R., Messina, A., Wagh, M., Fraulin, F.O.G., Morrison, W.A., and Stewart, A.G.: Inducible nitric oxide synthase (iNOS) activity promotes ischemic skin flap survival. *Br. J. Pharmacol.*, **132**, 1631-1638, 2001.

[45] Cuzzocrea, S., Chatterjee, P.K., Mazzon, E., Dugo, L., De Sarro, A., Van de Loo, F.A., Caputi, A.P., and Thiemermann, C.: Role of induced nitric oxide in the initiation of the inflammatory response after postischemic injury. *Shock*, 18, 169-176, 2002.

[46] Bolli, R.: Cardioprotective function of inducible nitric oxide synthase and role of nitric oxide in myocardial ischemia and preconditioning: an overview of a decade of research. *J. Mol. Cell. Cardiol.*, 33, 1897-918, 2001.

[47] Kisley, L.R., Barrett, B.S., Bauer, A.K., Dwyer-Nield, L.D., Barthel, B., Meyer, A.M., Thompson, D.C., and Malkinson, A.M.: Genetic ablation of inducible nitric oxide synthase decreases mouse lung Tumorigenesis. *Cancer. Res.*, **62**, 6850-6856 2002.

[48] Deininger, M.H., Wybranietz, W.A., Graepler, F.T., Lauer, U.M., Meyermann, R., and Schluesener, H.J.: Endothelial endostatin release is induced by general cell stress and modulated by the nitric oxide/cGMP pathway. *F.A.S.E.B. J.*, **17**, 1267-1276 2003.

[49] Cianchi, F., Cortesini, C., Fantappiè, O., Messerini, L., Sardi, I., Lasagna, N., Perna, F., Fabbroni, V., Felice, A.D., Perigli, G., Mazzanti, R., and Masini, E.: Cyclooxygenase-2 activation mediates the proangiogenic effect of nitric oxide in colorectal cancer. *Clin. Cancer. Res.*, **10**, 2694-2704, 2004.

[50] Fukumura, D., Gohongi, T., Kadambi, A., Izumi, Y., Ang, J., Yun, C.O., Buerk, D.G., Huang, P.L., and Jain, R.K.: Predominant role of endothelial nitric oxide synthase in vascular endothelial growth factor-induced angiogenesis and vascular permeability. *Proc. Natl. Acad. Sci. U. S. A.*, **98**, 2604-2609, 2001.

[51] Qi, W., Chen, L.E., Zhang, L., Eu, J.P., Seaber, A.V., and Urbaniak, J.R.: Reperfusion injury in skeletal muscle is reduced in inducible nitric oxide synthase knockout mice. *J. Appl. Physiol.*, **97**, 1323-1328, 2004.

Japanese Journal of Applied Physics
Vol. 45, No. 4A, 2006, pp. 2845–2849

Characteristic X-ray Generator Utilizing Angle Dependence of Bremsstrahlung X-ray Distribution

Eiichi SATO, Etsuro TANAKA[1], Hidezo MORI[2], Toshiaki KAWAI[3], Takashi INOUE[4], Akira OGAWA[4], Shigehiro SATO[5], Kazuyoshi TAKAYAMA[6] and Jun ONAGAWA[7]

Department of Physics, Iwate Medical University, 3-16-1 Honchodori, Morioka 020-0015, Japan
[1]*Department of Nutritional Science, Faculty of Applied Bio-science, Tokyo University of Agriculture, 1-1-1 Sakuragaoka, Setagaya-ku, Tokyo 156-8502, Japan*
[2]*Department of Cardiac Physiology, National Cardiovascular Center Research Institute, 5-7-1 Fujishirodai, Suita, Osaka 565-8565, Japan*
[3]*Electron Tube Division #2, Hamamatsu Photonics K.K., 314-5 Shimokanzo, Iwata, Shizuoka 438-0193, Japan*
[4]*Department of Neurosurgery, School of Medicine, Iwate Medical University, 19-1 Uchimaru, Morioka 020-8505, Japan*
[5]*Department of Microbiology, School of Medicine, Iwate Medical University, 19-1 Uchimaru, Morioka 020-8505, Japan*
[6]*Shock Wave Research Center, Institute of Fluid Science, Tohoku University, 2-1-1 Katahira, Sendai 980-8577, Japan*
[7]*Department of Applied Physics and Informatics, Faculty of Engineering, Tohoku Gakuin University, 1-13-1 Chuo, Tagajo, Miyagi 985-8537, Japan*

(Received November 17, 2005; revised December 24, 2005; accepted December 31, 2005; published online April 7, 2006)

This generator consists of the following components: a constant high-voltage power supply, a filament power supply, a turbomolecular pump, and an X-ray tube. The X-ray tube is a demountable diode which is connected to the turbomolecular pump and consists of the following major devices: a molybdenum rod target, a tungsten hairpin cathode (filament), a focusing (Wehnelt) electrode, a polyethylene terephthalate X-ray window 0.25 mm in thickness, and a stainless-steel tube body. In the X-ray tube, the positive high voltage is applied to the anode (target) electrode, and the cathode is connected to the tube body (ground potential). In this experiment, the tube voltage applied was from 22 to 36 kV, and the tube current was regulated to within 100 μA by the filament temperature. The exposure time is controlled in order to obtain optimum X-ray intensity. The electron beams from the cathode are converged to the target by the focusing electrode, and clean K-series characteristic X-rays are produced through the focusing electrode without using a filter. The X-ray intensity was 26.6 μGy/s at 1.0 m from the X-ray source with a tube voltage of 30 kV and a tube current of 100 μA, and quasi-monochromatic radiography was performed using a computed radiography system. [DOI: 10.1143/JJAP.45.2845]

KEYWORDS: demountable X-ray tube, electron-impact source, quasi-monochromatic X-rays, K-series characteristic X-rays, Sommerfeld's theory

1. Introduction

A great deal of effort has been devoted to the research and development of X-ray lasers in past years, and several different generators have been developed. Using tera-watt pulse lasers as pumping sources, a transient collisional excitation method has been proposed.[1] Subsequently, capillary discharge soft X-ray laser generators[2–4] have been developed and demonstrated. However, it is difficult to produce high-photon-energy X-ray lasers with energies 10 keV or beyond.

Recently, we have developed several different flash X-ray generators[5–9] corresponding to specific radiographic objectives, and the plasma X-ray source has been growing with increases in the electrostatic energy in the condenser. By forming weakly ionized linear plasma using rod targets, we confirmed irradiation of clean K-series characteristic X-rays such as hard X-ray lasers from the plasma axial direction using a table-top flash X-ray generator.[10–13] This super fluorescence has been employed to perform cone-beam monochromatic radiography such as iodine K-edge and gadolinium K-edge angiographies. Furthermore, because higher harmonic hard X-rays have been produced from the copper plasma, we have to confirm the irradiations of higher harmonics with charges in the target element.

Without forming plasmas, demountable flash X-ray tubes can be employed to perform fundamental study on producing monochromatic X-rays,[14] and have succeeded in producing clean K-series characteristic X-rays. However, monochromatic flash radiography has had difficulties in controlling X-ray duration, and in performing magnification radiography including phase-contrast effect.

At present, brilliant monochromatic parallel X-ray beams from synchrotron radiation are used in various fields including medical imaging,[15–17] and large-scale X-ray free electron laser sources[18] are constructing as a new-generation radiation source for producing monochromatic coherent X-rays. In contrast, small-scale steady-state monochromatic parallel and cone beams can be employed to perform medical imaging including phase-contrast radiography and K-edge angiography[19] in hospitals.

In this paper, we developed an X-ray generator used to perform a preliminary experiment for generating clean K-series characteristic X-rays by angle dependence of the bremsstrahlung X-rays.

2. Generator

Figure 1 shows a block diagram of a compact characteristic (quasi-monochromatic) X-ray generator. This generator consists of the following components: a constant high-voltage power supply (SL150, Spellman), a DC filament power supply, a turbomolecular pump, and an X-ray tube. The structure of the X-ray tube is illustrated in Fig. 2. The X-ray tube is a demountable diode which is connected to the turbomolecular pump with a pressure of approximately 0.5 mPa and consists of the following major devices: a molybdenum rod target of 3.0 mm in diameter, a tungsten hairpin cathode (filament), a focusing (Wehnelt) electrode, a polyethylene terephthalate X-ray window 0.25 mm in thickness, and a stainless-steel tube body. In the X-ray tube, the positive high voltage is applied to the anode (target) electrode, and the cathode is connected to the tube body

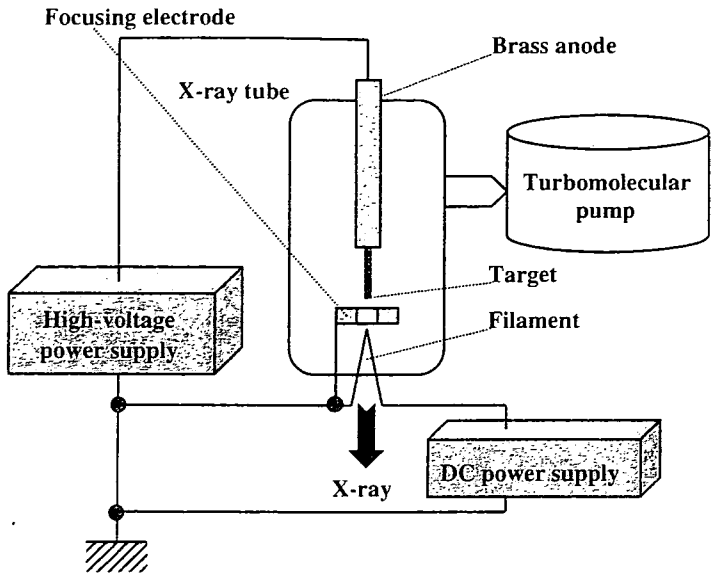

Fig. 1. Block diagram including the main transmission line of the compact X-ray generator with a quasi-monochromatic diode.

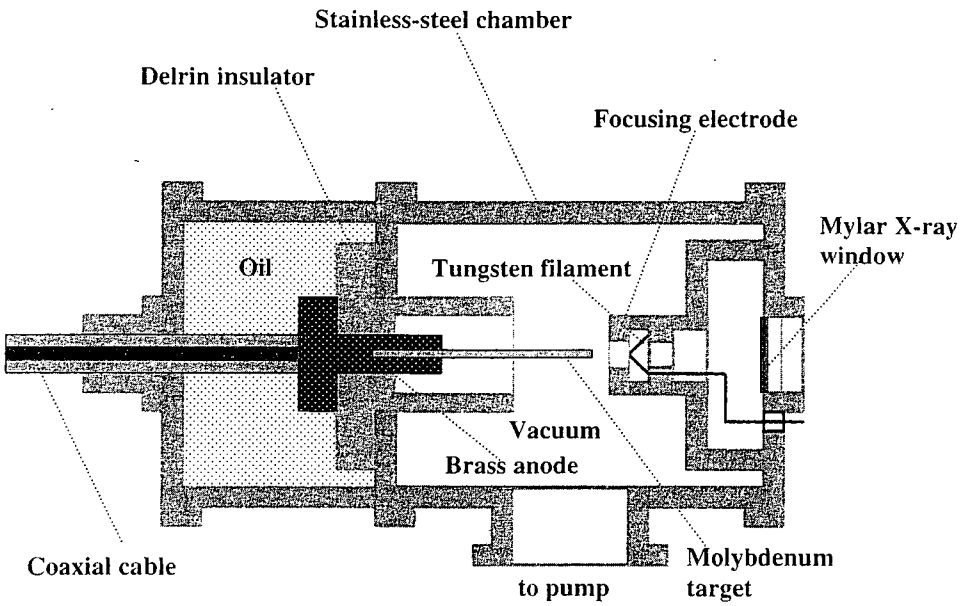

Fig. 2. Schematic drawing of the quasi-monochromatic X-ray tube.

(ground potential). In this experiment, the tube voltage applied was from 22 to 36 kV, and the tube current was regulated to within 100 μA by the filament temperature. The exposure time is controlled in order to obtain optimum X-ray intensity. The electron beams from the cathode are converged to the target by the focusing electrode, and X-rays are produced through the focusing electrode. Because bremsstrahlung rays are not emitted in the opposite direction to that of electron trajectory in Sommerfeld's theory[20] (Fig. 3), clean molybdenum K-series X-rays can be produced without using a filter.

3. Characteristics

3.1 X-ray intensity

X-ray intensity was measured by a Victoreen 660 ionization chamber at 1.0 m from the X-ray source (Fig. 4). At a constant tube current of 100 μA, the X-ray intensity increased when the tube voltage was increased. In this measurement, the intensity with a tube voltage of 30 kV and a current of 0.10 mA was 26.6 μGy/s at 1.0 m from the source.

3.2 X-ray source

In order to measure images of the X-ray source, we employed a pinhole camera with a hole diameter of 100 μm in conjunction with a computed radiography (CR) system[21] (Fig. 5). When the tube voltage was increased, the spot diameter slightly increased and had a maximum value of approximately 2.5 mm.

3.3 X-ray spectra

X-ray spectra were measured using a transmission-type spectrometer with a lithium fluoride curved crystal 0.5 mm in thickness. The X-ray intensities of the spectra were

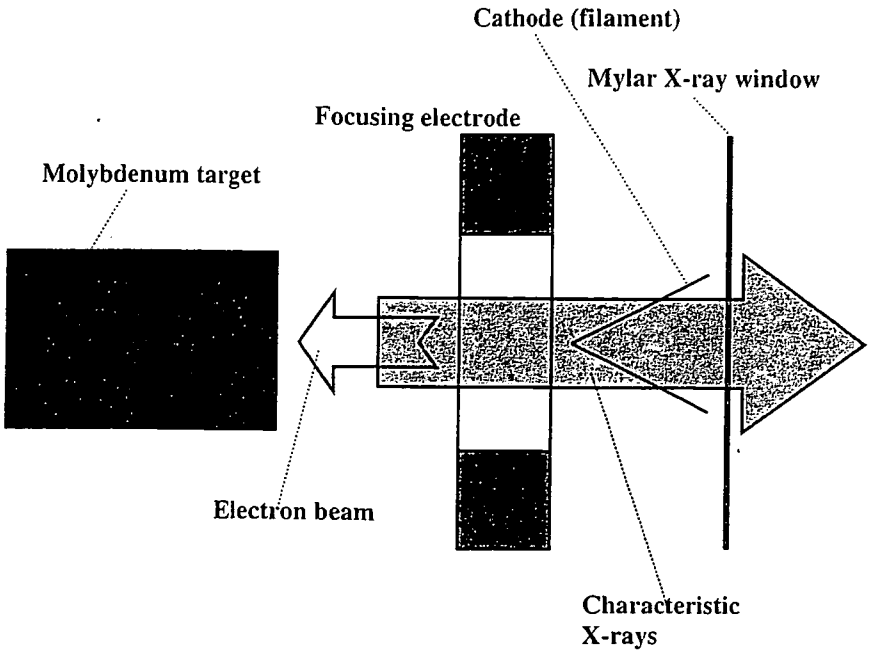

Fig. 3. K-photon irradiation from the X-ray tube.

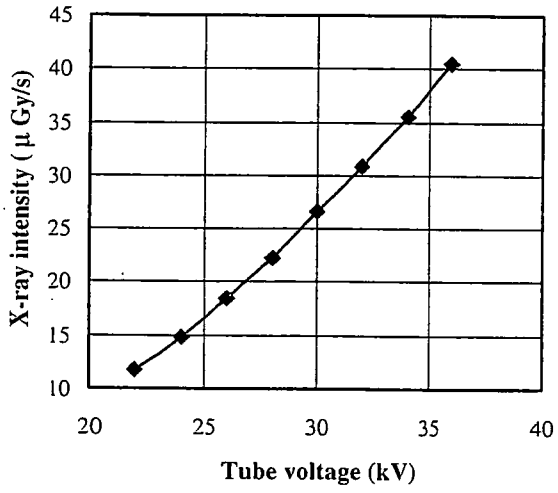

Fig. 4. X-ray intensity at 1.0 m from the X-ray source according to changes in the tube voltage with a tube current of 100 μA.

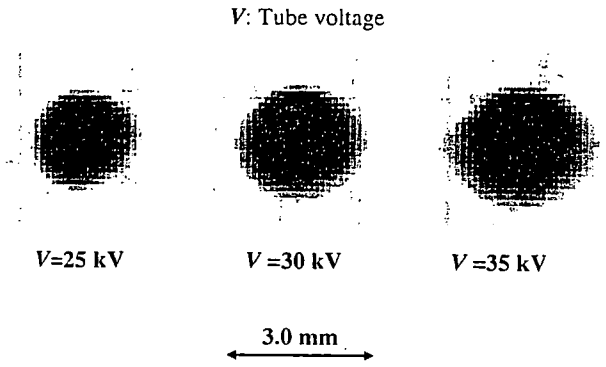

Fig. 5. Images of the characteristic X-ray source obtained using a pinhole camera with changes in the tube voltage.

detected by an imaging plate of the CR system (Konica Minolta, Regius 150) with a wide dynamic range, and relative X-ray intensity was calculated from Dicom original digital data corresponding to X-ray intensity; the data was scanned by Dicom viewer in the film-less CR system. Subsequently, the relative X-ray intensity as a function of the data was calibrated using a conventional X-ray generator, and we confirmed that the intensity was proportional to the exposure time. Figure 6 shows measured spectra from the molybdenum target. We observed clean K lines, while bremsstrahlung rays were hardly detected. The characteristic X-ray intensity substantially increased with increases in the tube voltage.

4. Radiography

The quasi-monochromatic radiography was performed by the CR system at 1.0 m from the X-ray source with the filter, and the tube voltage was 30 kV.

Firstly, rough measurements of image resolution were made using wires. Figure 7 shows radiograms of tungsten wires coiled around pipes made of poly(methyl methacrylate) (PMMA). Although the image contrast increased with increases in the wire diameter, a 50 μm-diameter wire could be observed.

A radiogram of a vertebra is shown in Fig. 8, and the fine structure of the vertebra was observed. Next, angiography was performed using iodine microspheres of 15 μm in diameter. Figures 9 and 10 show angiograms of a rabbit heart and thigh, respectively, and we could obtained high contrast images of coronary arteries and fine blood vessels.

5. Conclusions and Outlook

In summary, we developed a new quasi-monochromatic X-ray generator with a molybdenum-target tube and succeeded in producing clean molybdenum K lines. The characteristic X-ray intensity increased with increases in the tube voltage, and monochromatic Kα rays were left by a zirconium filter.

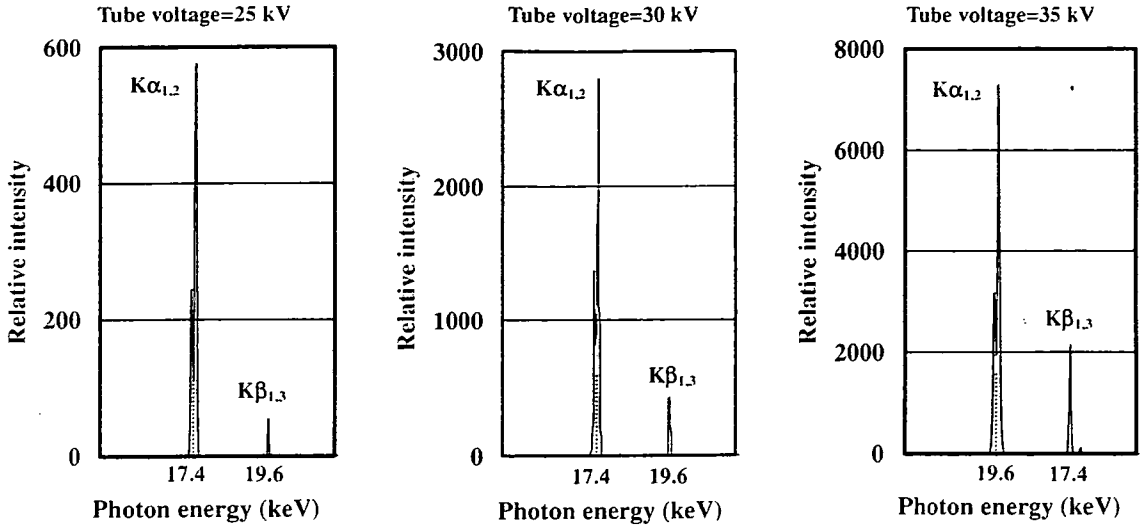

(a)

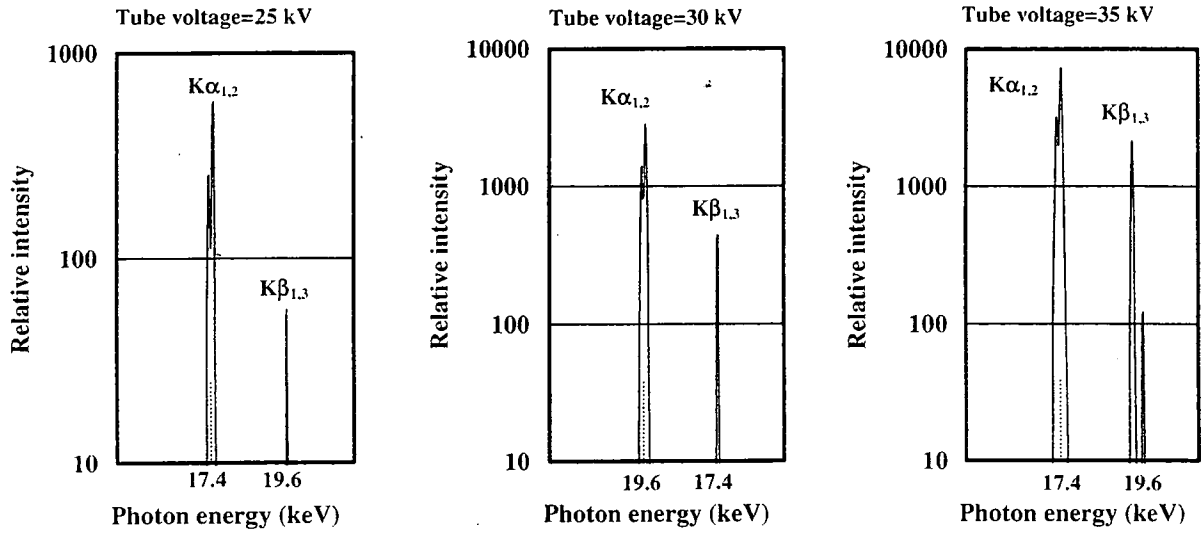

(b)

Fig. 6. X-ray spectra from the molybdenum target with (a) an ordinate scale and (b) a logarithmic scale. The spectra were measured using a transmission type spectrometer with a lithium fluoride curved crystal.

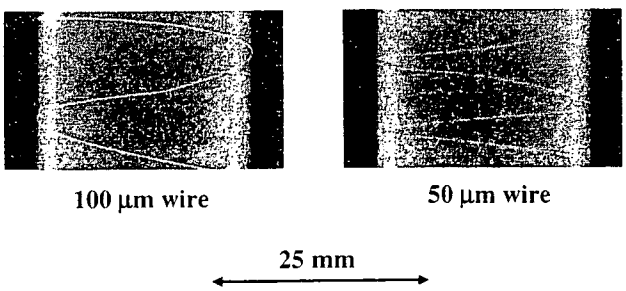

Fig. 7. Radiograms of tungsten wires of 50 and 100 μm in diameter coiled around pipes made of polymethyl methacrylate.

In this preliminary experiment, although the maximum tube voltage and current were 36 kV and 0.10 mA, the voltage and current could be increased to 100 kV and 1.0 mA, respectively. Under the pulsed operation, the current can be increased to approximately 1 A without considering

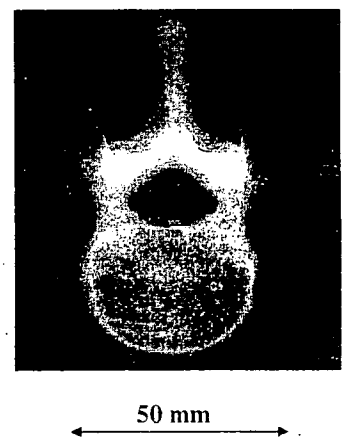

Fig. 8. Radiogram of a vertebra. Fine structure of the vertebra were visible.

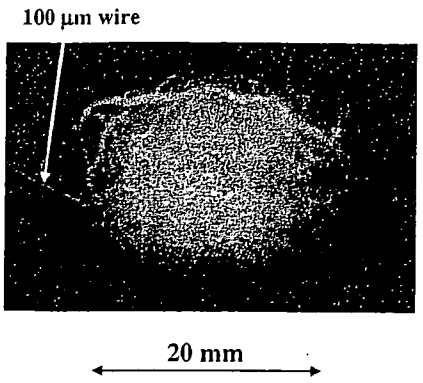

Fig. 9. Angiograms of a rabbit heart. Coronary arteries were visible.

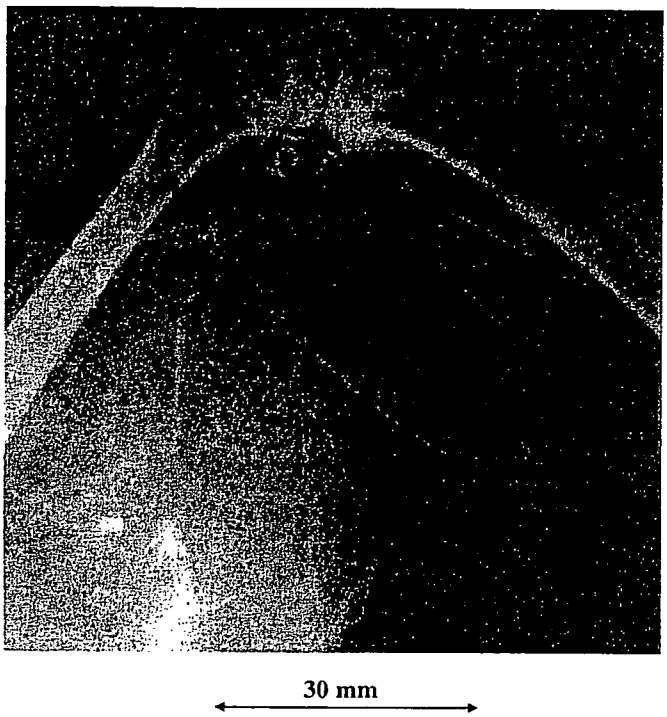

Fig. 10. Angiogram of a rabbit thigh. Fine blood vessels of approximately 100 μm were visible.

the target evaporation. Subsequently, the generator produced maximum number of characteristic photons was approximately 1×10^8 photons/(cm^2·s) at 1.0 m from the source, and the photon count rate can be increased easily by increasing the current.

In the present research, the molybdenum K-series characteristic X-rays are useful for mammography, and the photon energies of characteristic X-rays can be selected by the target element. In particular, enhanced K-edge angiography can be performed using a cerium target because cerium Kα rays (34.6 keV) are absorbed easily by iodine-based contrast media with an iodine K-edge of 33.2 keV. Using this angiography, coronary arteries and fine blood vessels formed in regenerative medicine may be observed with high contrasts. Furthermore, a flat panel detector is useful to observe blood flows for cases of cardiovascular disease.

Acknowledgment

This work was supported by Grants-in-Aid for Scientific Research (13470154, 13877114, and 16591222) and Advanced Medical Scientific Research from MECSST, Grants from Keiryo Research Foundation, The Promotion and Mutual Aid Corporation for Private School of Japan, JST (Test of Fostering Potential), NEDO, and MHLW (HLSRG, RAMT-nano-001, RHGTEFB-genome-005, and RGCD13C-1).

1) K. Nagashima, M. Tanaka, M. Nishikino, M. Kishimoto, M. Kado, T. Kawachi, N. Hasegawa, Y. Ochi, K. Sukegawa, R. Tai and K. Kato: Proc. SPIE **5197** (2003) 1.
2) J. J. Rocca, V. Shlyaptsev, F. G. Tomasel, O. D. Cortazar, D. Hartshorn and J. L. A. Chilla: Phys. Rev. Lett. **73** (1994) 2192.
3) C. D. Macchietto, B. R. Benware and J. J. Rocca: Opt. Lett. **24** (1999) 1115.
4) J. J. G. Rocca, J. L. A. Chilla, S. Sakadzic, A. Rahman, J. Filevich, E. Jankowska, E. C. Hammarsten, B. M. Luther, H. C. Kapteyn, M. Murnane and V. N. Shlyapsev: Proc. SPIE **4505** (2001) 1.
5) E. Sato, S. Kimura, S. Kawasaki, H. Isobe, K. Takahashi, Y. Tamakawa and T. Yanagisawa: Rev. Sci. Instrum. **61** (1990) 2343.
6) K. Takahashi, E. Sato, M. Sagae, T. Oizumi, Y. Tamakawa and T. Yanagisawa: Jpn. J. Appl. Phys. **33** (1994) 4146.
7) E. Sato, K. Takahashi, M. Sagae, S. Kimura, T. Oizumi, Y. Hayasi, Y. Tamakawa and T. Yanagisawa: Med. Biol. Eng. Comput. **32** (1994) 289.
8) E. Sato, M. Sagae, K. Takahashi, A. Shikoda, T. Oizumi, Y. Hayasi, Y. Tamakawa and T. Yanagisawa: Med. Biol. Eng. Comput. **32** (1994) 295.
9) E. Sato, E. Tanaka, H. Mori, T. Kawai, T. Ichimaru, S. Sato, K. Takayama and H. Ido: Med. Phys. **32** (2005) 49.
10) E. Sato, Y. Hayasi, R. Germer, E. Tanaka, H. Mori, T. Kawai, T. Ichimaru, K. Takayama and H. Ido: Rev. Sci. Instrum. **74** (2003) 5236.
11) E. Sato, Y. Hayasi, R. Germer, E. Tanaka, H. Mori, T. Kawai, T. Ichimaru, S. Sato, K. Takayama and H. Ido: J. Electron Spectrosc. Relat. Phenom. C **137–140** (2004) 713.
12) E. Sato, E. Tanaka, H. Mori, T. Kawai, S. Sato and K. Takayama: Opt. Eng. **44** (2005) 049002.
13) E. Sato, R. Germer, E. Tanaka, H. Mori, T. Kawai, T. Ichimaru, S. Sato, H. Ojima, K. Takayama and H. Ido: Proc. SPIE **5580** (2005) 146.
14) E. Sato, M. Sagae, E. Tanaka, Y. Hayasi, R. Germer, H. Mori, T. Kawai, T. Ichimaru, S. Sato, K. Takayama and H. Ido: Jpn. J. Appl. Phys. **43** (2004) 7324.
15) A. Momose, T. Takeda, Y. Itai and K. Hirano: Nat. Med. **2** (1996) 473.
16) H. Mori *et al.*: Radiology **201** (1996) 173.
17) K. Hyodo, M. Ando, Y. Oku, S. Yamamoto, T. Takeda, Y. Itai, S. Ohtsuka, Y. Sugishita and J. Tada: J. Synchrotron Radiat. **5** (1998) 1123.
18) K. Lan, E. E. Fill and J. M. Vehn: Proc. SPIE **5197** (2003) 253.
19) E. Sato, E. Tanaka, H. Mori, T. Kawai, T. Ichimaru, S. Sato, K. Takayama and H. Ido: Med. Phys. **31** (2004) 3017.
20) B. K. Agarwal: *X-ray Spectroscopy* (Springer-Verlag, New York, 1991) 2nd ed., p. 18.
21) E. Sato, K. Sato and Y. Tamakawa: Annu. Rep. Iwate Med. Univ. School Lib. Arts Sci. **35** (2000) 13.

Japanese Journal of Applied Physics
Vol. 45, No. 6A, 2006, pp. 5301–5306

X-ray Spectra from Weakly Ionized Linear Copper Plasma

Eiichi SATO, Yasuomi HAYASHI, Rudolf GERMER[1], Etsuro TANAKA[2], Hidezo MORI[3], Toshiaki KAWAI[4], Takashi INOUE[5], Akira OGAWA[5], Shigehiro SATO[6], Kazuyoshi TAKAYAMA[7] and Jun ONAGAWA[8]

Department of Physics, Iwate Medical University, 3-16-1 Honchodori, Morioka 020-0015, Japan
[1]*ITP, FHTW FB1 and TU-Berlin, Blankenhainer Str. 9, D 12249 Berlin, Germany*
[2]*Department of Nutritional Science, Faculty of Applied Bio-science, Tokyo University of Agriculture, 1-1-1 Sakuragaoka, Setagaya-ku, Tokyo 156-8502, Japan*
[3]*Department of Cardiac Physiology, National Cardiovascular Center Research Institute, 5-7-1 Fujishirodai, Suita, Osaka 565-8565, Japan*
[4]*Electron Tube Division #2, Hamamatsu Photonics K.K., 314-5 Shimokanzo, Iwata, Shizuoka 438-0193, Japan*
[5]*Department of Neurosurgery, School of Medicine, Iwate Medical University, 19-1 Uchimaru, Morioka 020-8505, Japan*
[6]*Department of Microbiology, School of Medicine, Iwate Medical University, 19-1 Uchimaru, Morioka 020-8505, Japan*
[7]*Shock Wave Research Center, Institute of Fluid Science, Tohoku University, 2-1-1 Katahira, Sendai 980-8577, Japan*
[8]*Department of Applied Physics and Informatics, Faculty of Engineering, Tohoku Gakuin University, 1-13-1 Chuo, Tagajo, Miyagi 985-8537, Japan*

(Received November 20, 2005; accepted April 5, 2006; published online June 8, 2006)

In the plasma flash X-ray generator, a 200 nF condenser is charged up to 50 kV by a power supply, and flash X-rays are produced by the discharging. The X-ray tube is a demountable triode with a trigger electrode, and the turbomolecular pump evacuates air from the tube with a pressure of approximately 1 mPa. Target evaporation leads to the formation of weakly ionized linear plasma, consisting of copper ions and electrons, around the fine target, and intense Kα lines are left using a 10-μm-thick nickel filter. At a charging voltage of 50 kV, the maximum tube voltage was almost equal to the charging voltage of the main condenser, and the peak current was about 16 kA. The K-series characteristic X-rays were clean and intense, and higher harmonic X-rays were observed. The X-ray pulse widths were approximately 300 ns, and the time-integrated X-ray intensity had a value of approximately 1.5 mGy per pulse at 1.0 m from the X-ray source with a charging voltage of 50 kV. [DOI: 10.1143/JJAP.45.5301]

KEYWORDS: linear plasma, X-ray spectra, K-series characteristic X-rays, bremsstrahlung X-rays, higher harmonic X-rays

1. Introduction

In order to produce X-ray lasers, several different methods have been developed, and a discharge capillary[1–3] is very useful to increase the laser pulse energy with increases in the capillary length. However, it is difficult to increase the laser photon energy to 10 keV or beyond.

Using monochrocollimators, synchrotrons produce monochromatic parallel beams, which are fairly similar to monochromatic parallel laser beams, and the beams have been applied to various research project including phase-contrast radiography[4,5] and enhanced K-edge angiography.[6,7] Because there are no X-ray resonators in the high-photon-energy region, new methods for increasing coherence will be desired in the future.

To apply flash X-ray generators to biomedicine, several different generators[8–13] have been developed, and plasma X-ray generators[14–17] are useful for producing clean characteristic X-rays in the low-photon-energy region of less than 10 keV. By forming weakly ionized linear plasma using rod targets, intense K-series characteristic X-rays are observed from the axial direction of the linear plasmas of nickel and copper, since the bremsstrahlung X-rays are absorbed effectively by the linear plasma. We are therefore very interested in the X-ray spectra produced by increasing the charging voltage in the high photon energy region beyond Kβ energies.

In this paper, we describe a recent table-top plasma flash X-ray generator utilizing a rod target triode, used to perform a preliminary experiment for generating clean K-series characteristic X-rays and their higher harmonic hard X-rays by forming a linear copper plasma cloud around a fine target.

2. Generator

Figure 1 shows a block diagram of the high-intensity plasma flash X-ray generator. This generator consists of the following essential components: a high-voltage power supply, a high-voltage condenser with a capacity of approximately 200 nF, a turbomolecular pump, a krytron pulse generator as a trigger device, and a flash X-ray tube. The high-voltage main condenser is charged to 50 kV by the power supply, and electric charges in the condenser are discharged to the tube after triggering the cathode electrode with the trigger device. The plasma flash X-rays are then produced.

The X-ray tube is a demountable cold-cathode triode that is connected to the turbomolecular pump with a pressure of approximately 1 mPa. This tube consists of the following major parts: a hollow cylindrical carbon cathode with a bore diameter of 10.0 mm, a brass focusing electrode, a trigger electrode made from copper wire, a stainless steel vacuum chamber, a nylon insulator, a poly(ethylene terephthalate) (Mylar) X-ray window 0.25 mm in thickness, and a rod-shaped copper target 3.0 mm in diameter with a tip angle of 60°. The distance between the target and cathode electrodes is approximately 20 mm, and the trigger electrode is set in the cathode electrode. As electron beams from the cathode electrode are roughly converged to the target by the focusing electrode, evaporation leads to the formation of a weakly ionized linear plasma,[18] consisting of copper ions and electrons, around the fine target.

In the linear plasma, bremsstrahlung photons with energies higher than the K-absorption edge are effectively absorbed and are converted into fluorescent X-rays. The plasma then transmits the fluorescent rays easily, and bremsstrahlung rays with energies lower than the K-edge

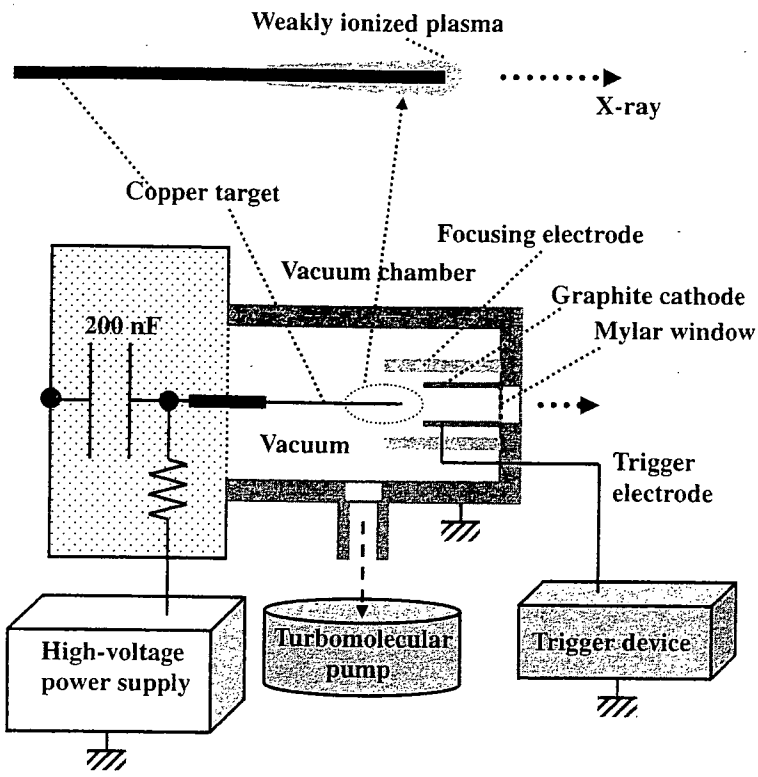

Fig. 1. Block diagram including the electric circuit of the plasma flash X-ray generator.

are also absorbed by the plasma. In addition, because bremsstrahlung rays are not emitted in the opposite direction to that of electron trajectory, intense characteristic X-rays are generated from the plasma-axial direction.

3. Characteristics

3.1 Tube voltage and current

Tube voltage and current were measured by a high-voltage divider with an input impedance of 1 GΩ and a current transformer, respectively. The withstand voltage of the divider is approximately 60 kV, and the measurable current of the transformer ranges from 1 A to 100 kA. Figure 2 shows the time relation between the tube voltage and current. At the indicated charging voltages, they roughly displayed damped oscillations. When the charging voltage was increased, both the maximum tube voltage and current increased. At a charging voltage of 50 kV, the maximum tube voltage was almost equal to the charging voltage of the main condenser, and the maximum tube current was approximately 16 kA.

3.2 X-ray output

X-ray output pulse was detected using a combination of a plastic scintillator and a photomultiplier (Fig. 3). The X-ray pulse height substantially increased with corresponding increases in the charging voltage. The rise time increased with increasing the voltage because the K-series characteristic X-rays were produced with tube voltages beyond the critical excitation voltage of 8.9 kV. The X-ray pulse widths were about 300 ns, and the time-integrated X-ray intensity per pulse measured by a thermoluminescence dosimeter (Kyokko TLD Reader 1500 having MSO-S elements without energy compensation) had a value of approximately 1.5 mGy at 1.0 m from the X-ray source with a charging voltage of 50 kV. The TLD reader has a wide measurable range of from 1 μSv to 100 Sv.

3.3 X-ray source

In order to roughly observe images of the plasma X-ray source in the detector plane, we employed a pinhole camera with a hole diameter of 100 μm without using a filter (Fig. 4). When the charging voltage was increased, the plasma X-ray source grew, and both spot dimension and intensity increased. Because the X-ray intensity is the highest at the center of the spot, both the dimension and intensity decreased according to both increases in the thickness of a filter for absorbing X-rays and decreases in the pinhole diameter.

3.4 X-ray spectra

X-ray spectra from the plasma source were measured by a transmission-type spectrometer with a lithium fluoride curved crystal 0.5 mm in thickness. The spectra were taken by a computed radiography (CR) system[19] (Konica Minolta, Regius 150) with a wide dynamic range beyond five figures for measuring X-ray intensity, and relative X-ray intensity was calculated from Dicom digital data. Subsequently, the relative X-ray intensity as a function of the data was calibrated using a conventional X-ray generator, and we confirmed that the intensity was proportional to the exposure time. Figure 5 shows measured spectra from the copper target at the indicated conditions. In fact, we observed clean K lines, and Kα lines were left by absorbing Kβ lines using a 10-μm-thick nickel filter. When the charging voltage was increased, the characteristic X-ray intensity substantially increased. In particular, we confirmed the irradiation of

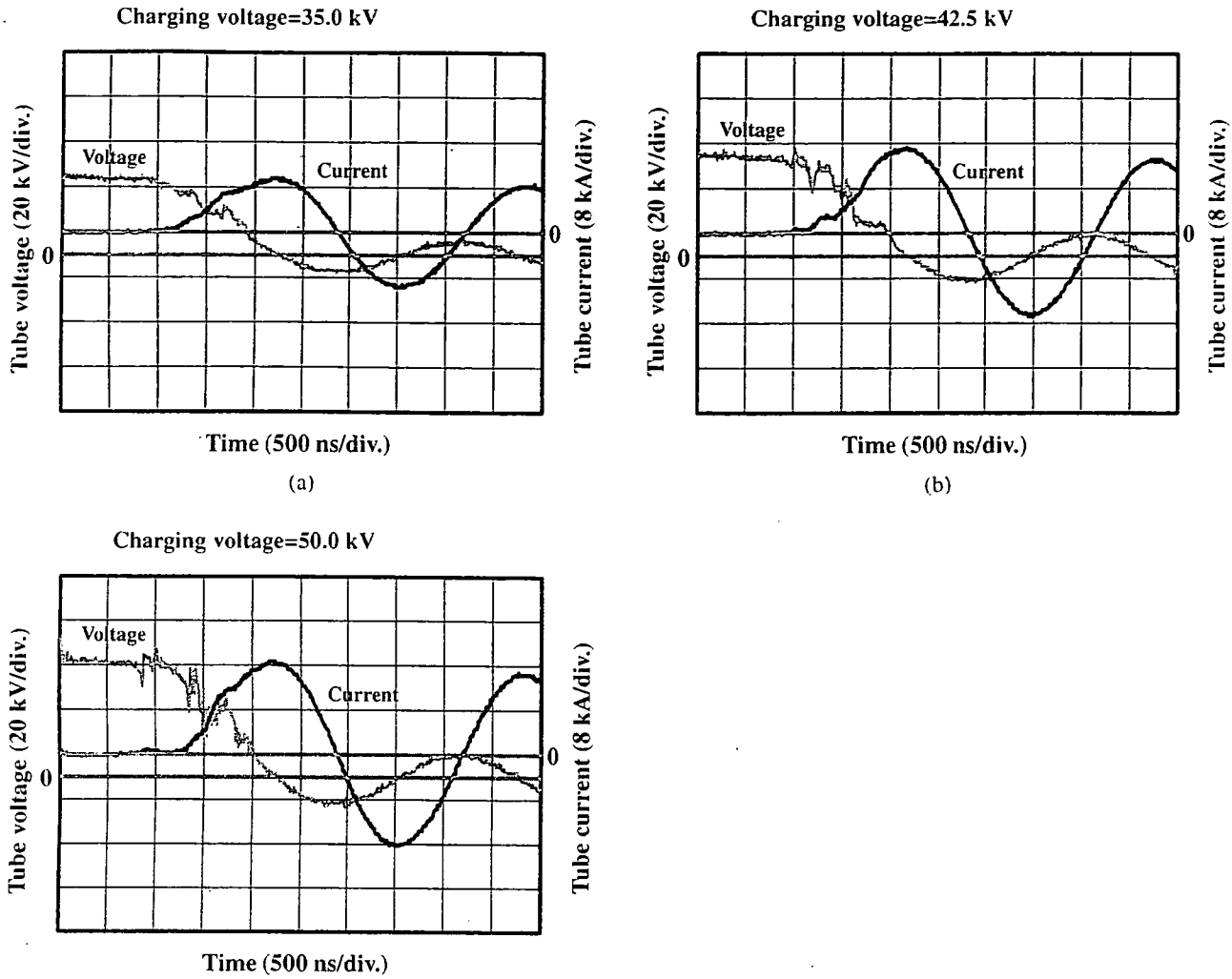

Fig. 2. Tube voltages and currents with a charging voltage of (a) 35.0, (b) 42.5, and (b) 50.0 kV.

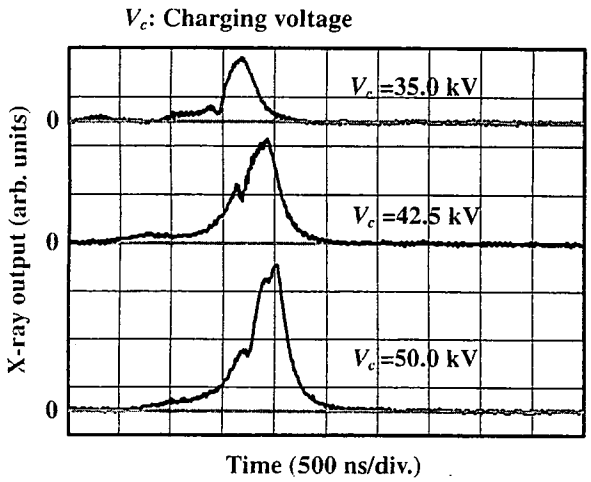

Fig. 3. X-ray outputs at the indicated conditions.

the second and fourth harmonic X-rays of the fundamental K-series characteristic X-rays from copper target. The X-ray intensities of the harmonics increased with increases in the charging voltage, and the harmonic bremsstrahlung rays survived due to the X-ray resonation in the plasma.

4. Radiography

The plasma radiography was performed by the CR system using the filter. The charging voltage and the distance between the X-ray source and imaging plate were 50 kV and 1.2 m, respectively. First, rough measurements of spatial resolution were made using wires. Figure 6 shows radiograms of tungsten wires coiled around pipes made of poly(methyl methacrylate) (PMMA). Although the image contrast decreased somewhat with decreases in the wire diameter, due to blurring of the image caused by the sampling pitch of 87.5 μm, a 50-μm-diameter wire could be observed.

Figure 7 shows a radiogram of plastic bullets falling into a polypropylene beaker from a plastic test tube. Because the X-ray duration was about 0.5 μs, the stop-motion image of bullets could be obtained. Next, a radiogram of a vertebra is shown in Fig. 8, and fine structures in the vertebra were observed. Finally, Fig. 9 shows an angiogram of a rabbit ear: iodine-based microspheres of 15 μm in diameter were used, and fine blood vessels of about 100 μm were visible.

5. Conclusions and Outlook

We obtained fairly intense and clean K lines from a weakly ionized linear copper plasma, and Kα lines were left

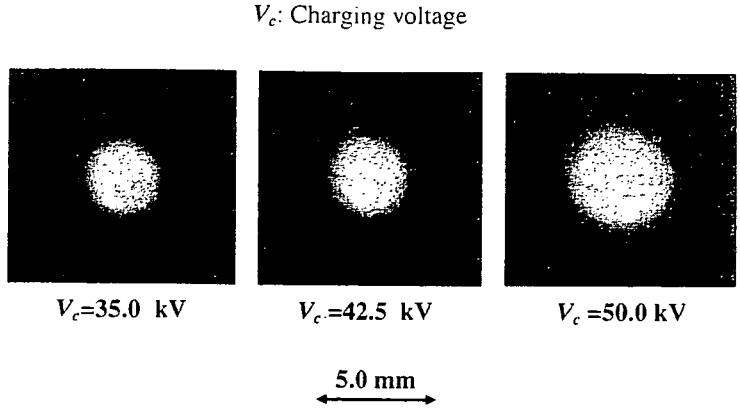

Fig. 4. Images of the plasma X-ray source.

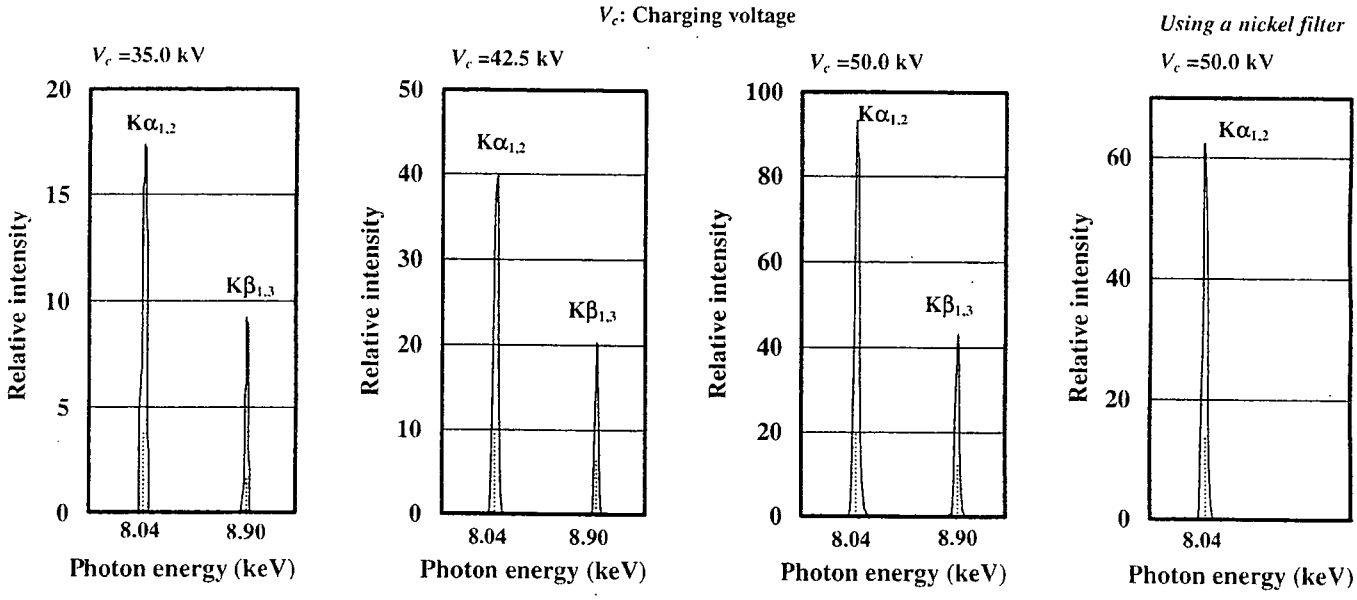

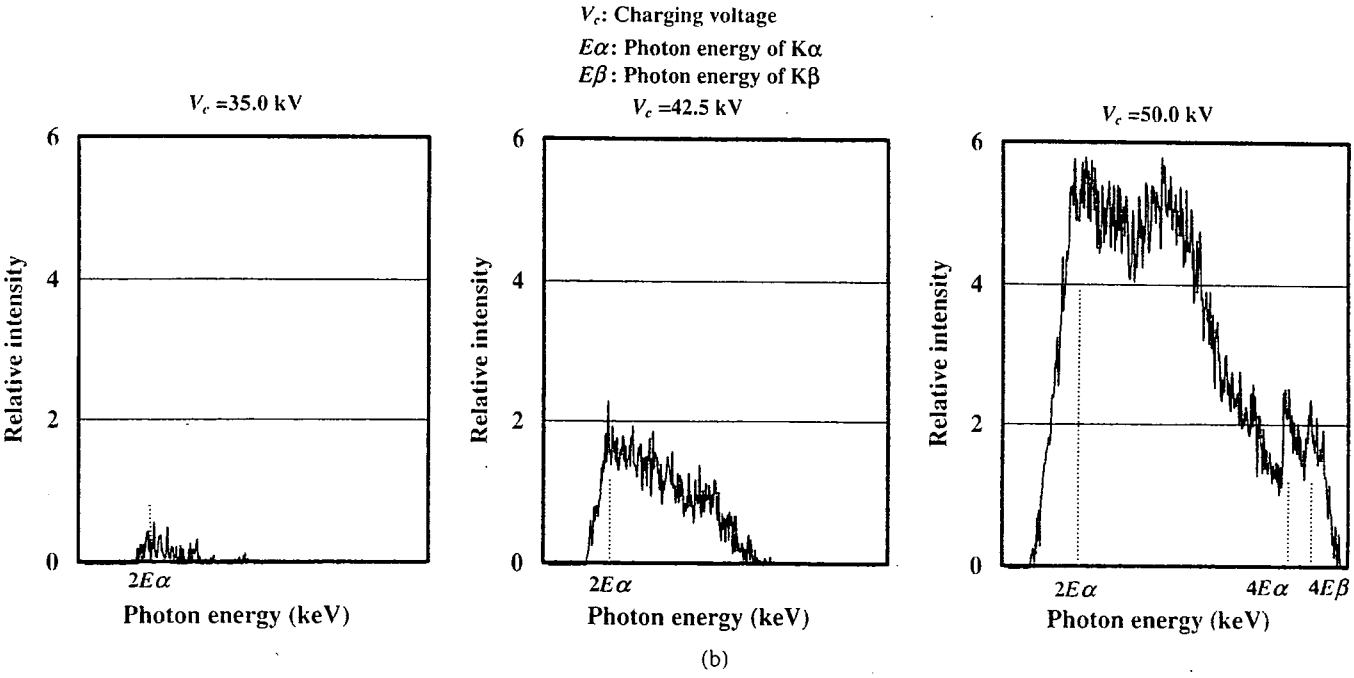

Fig. 5. X-ray spectra from weakly ionized copper plasma at the indicated conditions. (a) characteristic X-rays and (b) higher harmonic X-rays.

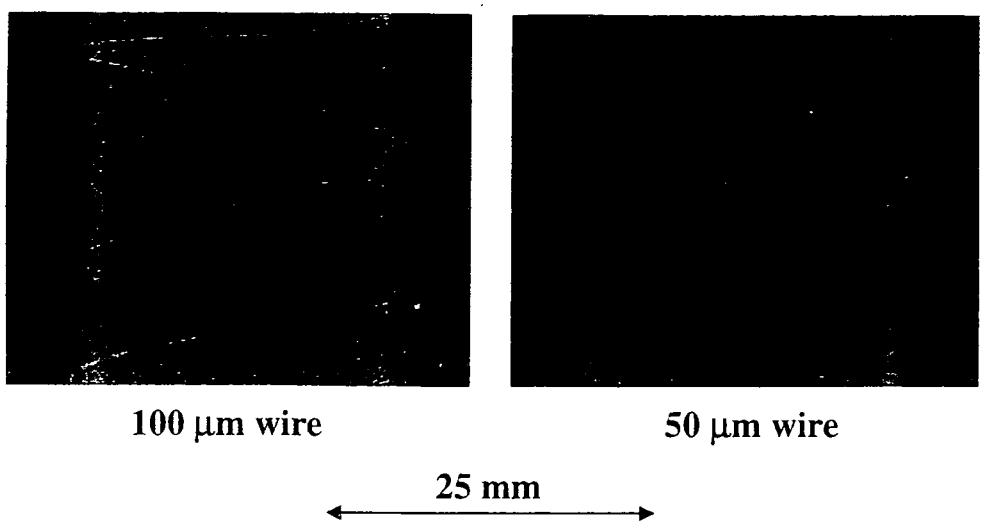

Fig. 6. Radiograms of tungsten wires coiled around PMMA pipes.

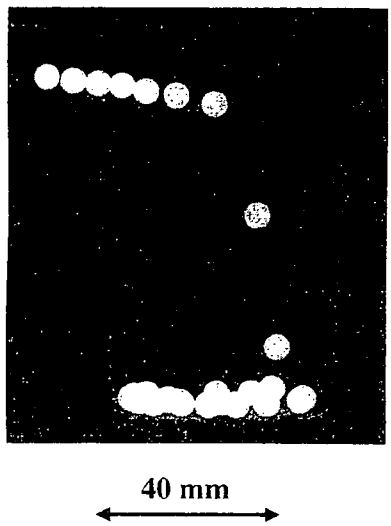

Fig. 7. Radiogram of plastic bullets falling into polypropylene beaker from a plastic test tube.

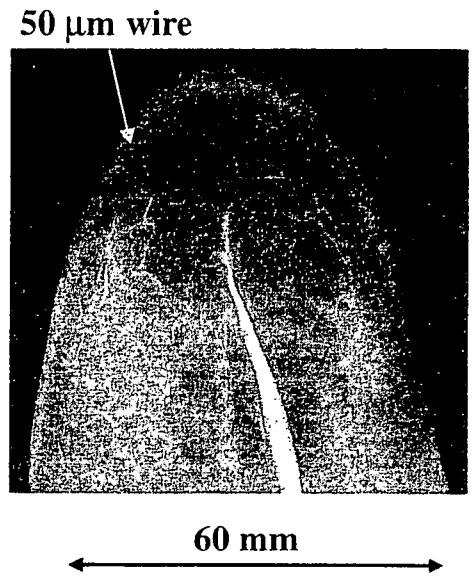

Fig. 9. Angiogram of a rabbit ear.

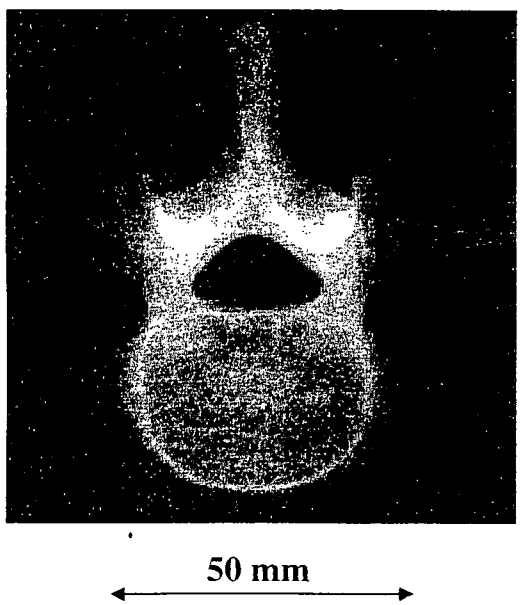

Fig. 8. Radiogram of a vertebra.

by the nickel filter. Both the characteristic and the harmonic X-ray intensities substantially increased with increasing the charging voltage.

In cases where weakly ionized linear plasma is employed, intense and clean K-series characteristic X-rays can be obtained. However, it is not easy to produce high-photon-energy K-series characteristic X-rays because the linear plasma transmits high-photon-energy bremsstrahlung X-rays; the effective thickness of a monochromatic metal filter increases with increases in the atomic number. Therefore, high-photon-energy plasma flash X-ray generators utilizing the angle dependence of bremsstrahlung X-rays are very useful to produce K photons of molybdenum, silver, cerium, tantalum, and tungsten. In particular, Kα rays of tantalum and tungsten are useful for performing enhanced K-edge angiography using gadolinium contrast media, and cerium K rays can be employed to perform iodine K-edge angiography.

In this research, we obtained sufficient characteristic X-ray intensity per pulse for CR radiography, and the

generator produced number of characteristic K photons was approximately 1×10^8 photons/cm^2 at 1.0 m per pulse. In addition, we are very interested in producing steady-state clean K rays and their higher harmonic hard X-rays using a similar tube.

Acknowledgments

This work was supported by Grants-in-Aid for Scientific Research (13470154, 13877114, 16591181, and 16591222) and Advanced Medical Scientific Research from MECSST, Health and Labor Sciences Research Grants (RAMT-nano-001, RHGTEFB-genome-005 and RHGTEFB-saisei-003), Grants from The Keiryo Research Foundation, The Promotion and Mutual Aid Corporation for Private Schools of Japan, Japan Science and Technology Agency (JST), and the New Energy and Industrial Technology Development Organization (NEDO, Industrial Technology Research Grant Program in '03).

1) J. J. Rocca, V. Shlyaptsev, F. G. Tomasel, O. D. Cortazar, D. Hartshorn and J. L. A. Chilla: Phys. Rev. Lett. **73** (1994) 2192.
2) C. D. Macchietto, B. R. Benware and J. J. Rocca: Opt. Lett. **24** (1999) 1115.
3) J. J. G. Rocca, J. L. A. Chilla, S. Sakadzic, A. Rahman, J. Filevich, E. Jankowska, E. C. Hammarsten, B. M. Luther, H. C. Kapteyn, M. Murnane and V. N. Shlyapsev: Proc. SPIE **4505** (2001) 1.
4) A. Momose, T. Takeda, Y. Itai and K. Hirano: Nat. Med. **2** (1996) 473.
5) M. Ando, A. Maksimenko, H. Sugiyama, W. Pattanasiriwisawa, K. Hyodo and C. Uyama: Jpn. J. Appl. Phys. **41** (2002) L1016.
6) H. Mori *et al.*: Radiology **201** (1996) 173.
7) K. Hyodo, M. Ando, Y. Oku, S. Yamamoto, T. Takeda, Y. Itai, S. Ohtsuka, Y. Sugishita and J. Tada: J. Synchrotron Radiat. **5** (1998) 1123.
8) E. Sato, S. Kimura, S. Kawasaki, H. Isobe, K. Takahashi, Y. Tamakawa and T. Yanagisawa: Rev. Sci. Instrum. **61** (1990) 2343.
9) K. Takahashi, E. Sato, M. Sagae, T. Oizumi, Y. Tamakawa and T. Yanagisawa: Jpn. J. Appl. Phys. **33** (1994) 4146.
10) E. Sato, K. Takahashi, M. Sagae, S. Kimura, T. Oizumi, Y. Hayasi, Y. Tamakawa and T. Yanagisawa: Med. Biol. Eng. Comput. **32** (1994) 289.
11) E. Sato, M. Sagae, K. Takahashi, A. Shikoda, T. Oizumi, Y. Hayasi, Y. Tamakawa and T. Yanagisawa: Med. Biol. Eng. Comput. **32** (1994) 295.
12) E. Sato, M. Sagae, E. Tanaka, Y. Hayasi, R. Germer, H. Mori, T. Kawai, T. Ichimaru, S. Sato, K. Takayama and H. Ido: Jpn. J. Appl. Phys. **43** (2004) 7324.
13) E. Sato, E. Tanaka, H. Mori, T. Kawai, T. Ichimaru, S. Sato, K. Takayama and H. Ido: Med. Phys. **32** (2005) 49.
14) E. Sato, Y. Hayasi, R. Germer, E. Tanaka, H. Mori, T. Kawai, H. Obara, T. Ichimaru, K. Takayama and H. Ido: Jpn. J. Med. Phys. **23** (2003) 123.
15) E. Sato, Y. Hayasi, R. Germer, E. Tanaka, H. Mori, T. Kawai, T. Ichimaru, K. Takayama and H. Ido: Rev. Sci. Instrum. **74** (2003) 5236.
16) E. Sato, Y. Hayasi, R. Germer, E. Tanaka, H. Mori, T. Kawai, T. Ichimaru, S. Sato, K. Takayama and H. Ido: J. Electron Spectrosc. Relat. Phenom. C **137–140** (2004) 713.
17) E. Sato, E. Tanaka, H. Mori, T. Kawai, S. Sato and K. Takayama: Opt. Eng. **44** (2005) 049002.
18) E. Sato, M. Sagae, K. Takahashi, T. Ichimaru, W. Aiba, S. Kumagai, Y. Hayasi, H. Ido, K. Sakamaki, K. Takayama and Y. Tamakawa: Proc. SPIE **3336** (1998) 75.
19) E. Sato, K. Sato and Y. Tamakawa: Ann. Rep. Iwate Med. Univ. Sch. Lib. Arts Sci. **35** (2000) 13.

Japanese Journal of Applied Physics
Vol. 45, No. 10A, 2006, pp. 8005–8009

Enhanced Magnification Angiography Using 20-μm-Focus Tungsten Tube

Toshiyuki ENOMOTO, Eiichi SATO[1], Yoshinobu SUMIYAMA, Katsuo AIZAWA[2], Manabu WATANABE, Etsuro TANAKA[3], Hidezo MORI[4], Hiroki KAWAKAMI[5], Toshiaki KAWAI[5], Takashi INOUE[6], Akira OGAWA[6] and Shigehiro SATO[7]

The 3rd Department of Surgery, Toho University School of Medicine, 2-17-6 Ohashi, Meguro-ku, Tokyo 153-8515, Japan
[1]*Department of Physics, Iwate Medical University, 3-16-1 Honchodori, Morioka 020-0015, Japan*
[2]*Tokyo Medical University [emeritus professor], 6-1-1 Shinjuku, Shinjuku-ku, Tokyo 160-8402, Japan*
[3]*Department of Nutritional Science, Faculty of Applied Bio-science, Tokyo University of Agriculture, 1-1-1 Sakuragaoka, Setagaya-ku, Tokyo 156-8502, Japan*
[4]*Department of Cardiac Physiology, National Cardiovascular Center Research Institute, 5-7-1 Fujishirodai, Suita, Osaka 565-8565, Japan*
[5]*Electron Tube Division #2, Hamamatsu Photonics K.K., 314-5 Shimokanzo, Iwata, Shizuoka 438-0193, Japan*
[6]*Department of Neurosurgery, School of Medicine, Iwate Medical University, 19-1 Uchimaru, Morioka 020-8505, Japan*
[7]*Department of Microbiology, School of Medicine, Iwate Medical University, 19-1 Uchimaru, Morioka 020-8505, Japan*

(Received April 10, 2006; accepted June 25, 2006; published online October 6, 2006)

A microfocus X-ray tube is useful for performing magnification radiography, and its X-ray generator (L9631, Hamamatsu Photonics) consists of a personal computer for controlling the tube voltage and current, and a main unit with a high-voltage circuit and a fixed-anode X-ray tube. The maximum tube voltage, current, and electric power were 110 kV, 800 μA, and 50 W, respectively. The focal-spot size was proportional to the electric power of the tube, and the size was approximately 20 μm with a power of 20 W. Using a 3-mm-thick aluminum filter, the X-ray intensity was 7.75 μGy/s at 1.0 m from the source with a tube voltage of 60 kV and a current of 100 μA. Because the peak photon energy was approximately 38 keV using the filter with a tube voltage of 60 kV, the bremsstrahlung X-rays were absorbed effectively by iodine-based contrast media at an iodine K-edge of 33.2 keV. Enhanced angiography was performed by fourfold magnification imaging with a computed radiography system using iodine-based microspheres 15 μm in diameter. In the angiography of nonliving animals, we observed fine blood vessels of approximately 100 μm with high contrast. [DOI: 10.1143/JJAP.45.8005]

KEYWORDS: high-contrast angiography, magnification digital radiography, microfocus X-ray tube, energy-selective imaging

1. Introduction

To perform high-speed medical radiography, several various flash X-ray generators using cold-cathode tubes have been developed.[1–4] In particular, quasi-monochromatic flash X-ray generators[5–10] have been designed to perform preliminary experiments for producing clean K-series X-rays, and higher-harmonic hard X-rays have been observed in a weakly ionized linear plasma of copper and nickel. However, in monochromatic flash radiography, difficulties in increasing X-ray duration and in performing X-ray computed tomography (CT) have been encountered.

Synchrotrons are capable of producing high-dose-rate monochromatic parallel X-ray beams using silicon crystals, and the beams have been applied to phase-contrast radiography[11,12] and enhanced K-edge angiography.[13,14] In angiography, monochromatic X-rays with photon energies ranging from 33.3 to 35 keV have been employed because the rays are absorbed effectively by iodine-based contrast media with an iodine K-edge of 33.2 keV.

Without using synchrotrons, phase-contrast radiography[15] for edge enhancement can be performed using a microfocus X-ray tube, and the enhancement has been achieved in mammography[16] with a computed radiography (CR) system[17] using a 100-μm-focus tube. Subsequently, we developed a cerium X-ray generator[18,19] to perform enhanced K-edge angiography using cone beams, and succeeded in observing fine blood vessels and coronary arteries with high contrast using cerium Kα-rays of 34.6 keV.

Although the magnification radiography is used to improve the spatial resolution in angiography utilizing a digital imaging system, it is difficult to design a small focus cerium tube for angiography. Therefore, narrow-photon-energy bremsstrahlung X-rays[20–22] with a peak energy of approximately 35 keV from a tungsten tube are used to perform high-contrast angiography.

In this research, we employed a microfocus tungsten tube, and performed enhanced magnification angiography by controlling bremsstrahlung X-ray spectra using an aluminum filter.

2. Principle of Enhanced Magnification Angiography

Figure 1 shows the mass attenuation coefficients of iodine at the selected energies; the coefficient curve is discontinuous at the iodine K-absorption edge of 33.2 keV. The effective bremsstrahlung X-rays for K-edge angiography are shown above the K-edge. Using a 3.0-mm-thick aluminum filter for absorbing soft X-rays, the peak photon energy of the bremsstrahlung rays increases to approximately 38 keV. In angiography, iodine contrast media in blood vessels easily absorb the rays, and soft bremsstrahlung rays are absorbed effectively by objects (muscles). Therefore, blood vessels are observed with high contrast. Subsequently, spatial resolution is improved by fourfold magnification imaging using a microfocus X-ray tube in conjunction with a CR system (Regius 150, Konica Minolta) at a sampling pitch of 87.5 μm.

3. Experimental Methods

The microfocus X-ray generator (L9631, Hamamatsu Photonics) consists of a personal computer and a system unit. The unit includes all the hardware in the X-ray generator, such as, a high-voltage circuit and a fixed anode X-ray tube. Tube voltage, current, and exposure time can be controlled by the computer. The maximum tube voltage, current, and electric power were 110 kV, 800 μA, and 50 W,

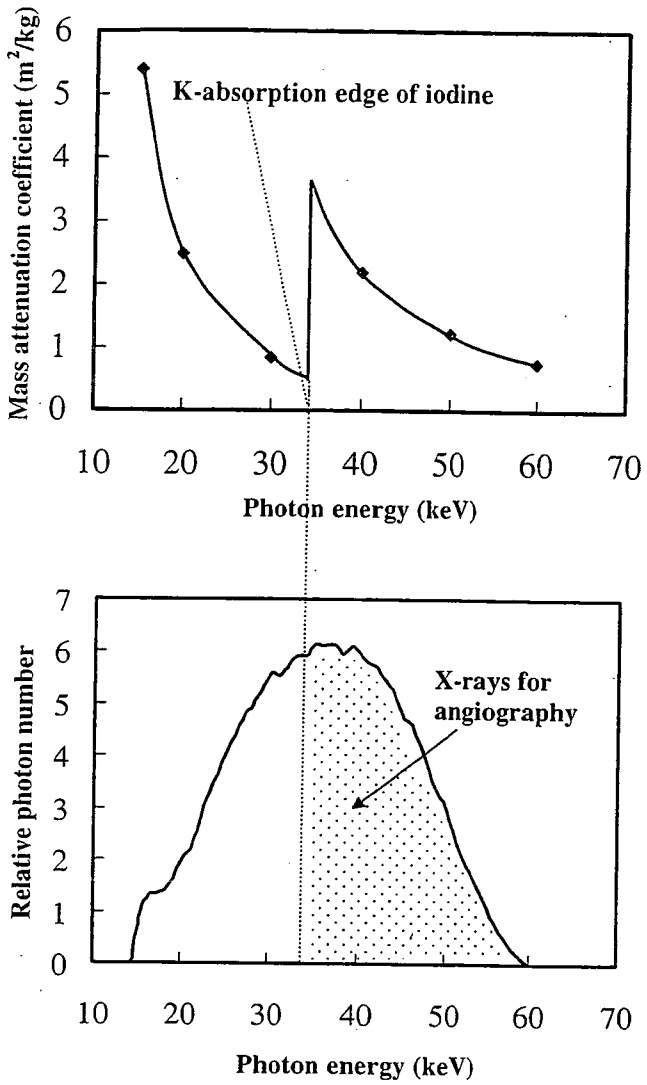

Fig. 1. Mass attenuation coefficients of iodine and bremsstrahlung X-rays for enhanced K-edge angiography.

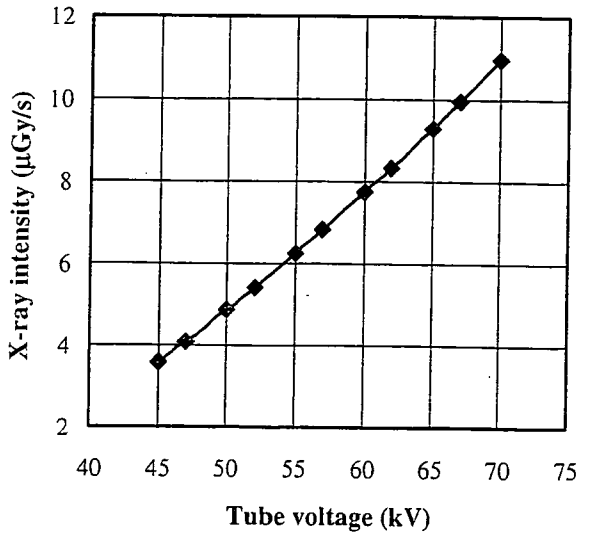

Fig. 2. X-ray intensity (μGy/s) as a function of tube voltage (kV) with tube current of 100 μA.

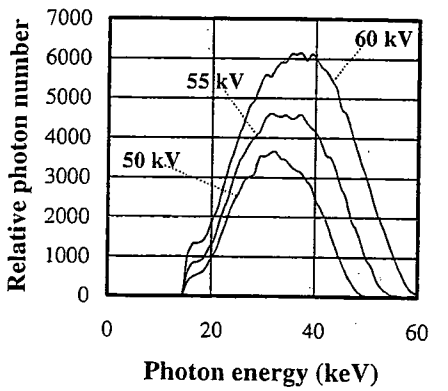

Fig. 3. Bremsstrahlung X-ray spectra measured using cadmium telluride detector with changes in tube voltage.

respectively. The focal-spot size was proportional to the electric power of the tube, and its size was approximately 20 μm in diameter with a power of 20 W. In this experiment, the tube voltage applied ranged from 45 to 70 kV, and the tube current was regulated to within 170 μA. The exposure time is controlled to obtain optimum X-ray intensity for angiography, and narrow-photon-energy bremsstrahlung X-rays are produced using the aluminum filter.

4. Results

4.1 X-ray intensity

X-ray intensity was measured using a Victoreen 660 ionization chamber, with a volume of 400 cm^3, at 1.0 m from the X-ray source using the filter (Fig. 2). At a constant tube current of 100 μA, X-ray intensity increased when tube voltage was increased. At a tube voltage of 60 kV, the X-ray intensity with the filter was 7.75 μGy/s.

4.2 X-ray spectra

To measure X-ray spectra using the filter, we employed a cadmium telluride detector (CDTE2020X, Hamamatsu Photonics) (Fig. 3). When tube voltage was increased, bremsstrahlung X-ray intensity increased, and both maximum photon energy and spectrum peak energy increased.

To perform K-edge angiography, bremsstrahlung X-rays of approximately 35 keV are used; the high-energy bremsstrahlung X-rays decrease image contrast. When this filter was used, because bremsstrahlung X-rays with energies higher than 60 keV were not absorbed easily, the tube voltage for angiography was determined to be 60 kV by considering the filtering effect of radiographic objects.

4.3 Enhanced magnification angiography

The enhanced angiography was performed by fourfold magnification imaging using the CR system and the filter at a tube voltage of 60 kV, and the distance between the X-ray source and the imaging plate was 1.0 m (Fig. 4). First, the spatial resolutions of cohesion and magnification radiographies were realized using a lead test chart at an exposure time of 30 s. In the magnification radiography, 50-μm-thick lines (10 line pairs) were clearly visible (Fig. 5). Figure 6 shows radiograms of tungsten wires in a 25-mm-diameter rod made of poly(methyl methacrylate) (PMMA) at an exposure time of 30 s. Although image contrast decreased slightly with decreasing wire diameter owing to the blurring of the image caused by the sampling pitch of 87.5 μm, a 20-μm-diameter wire could be observed.

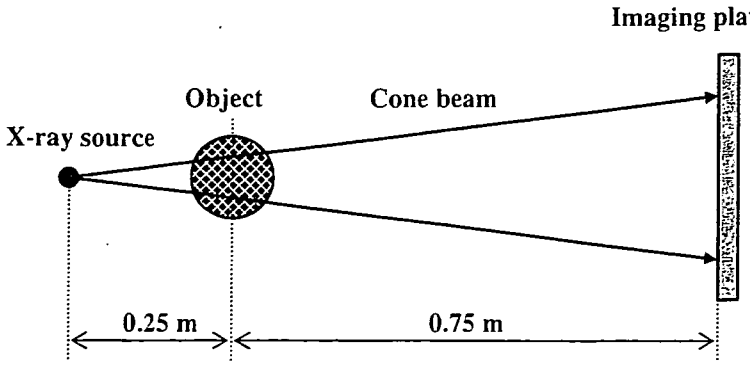

Fig. 4. Fourfold magnification imaging using imaging plate in conjunction with microfocus tube.

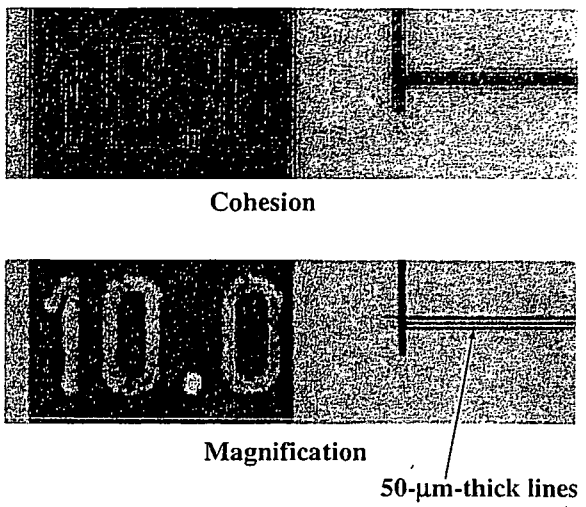

Fig. 5. Radiogram of test chart for measuring spatial resolution.

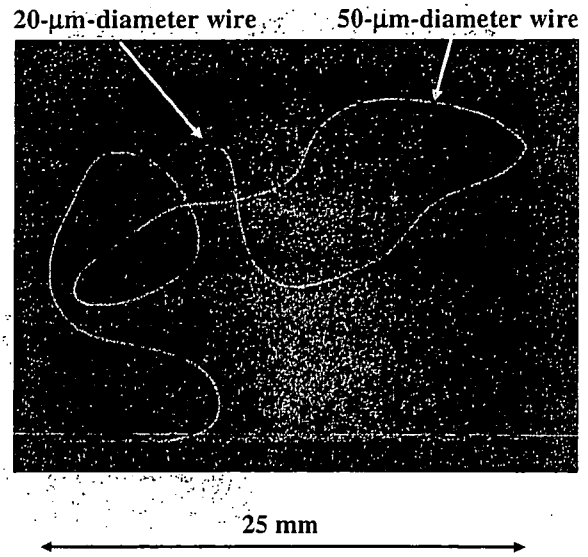

Fig. 6. Radiograms of tungsten wires in PMMA rod.

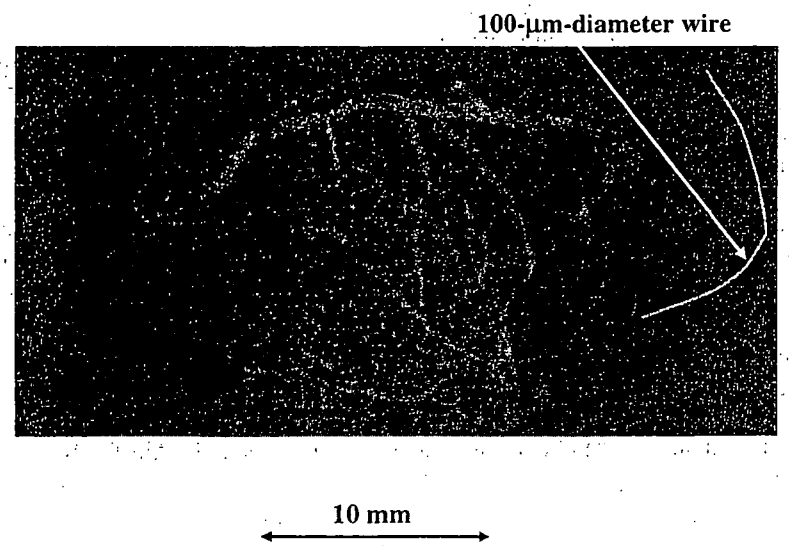

Fig. 7. Angiogram of extracted rabbit heart using iodine microspheres.

Figures 7 and 8 show angiograms of a 19-mm-thick rabbit heart specimen and a 41-mm-thick thigh specimen, respectively. The exposure time was 30 s, and these images were obtained using iodine microspheres of 15 μm diameter. The microspheres are very useful for making the phantoms of nonliving animals used for angiography. The iodine plastic spheres contained 37% iodine by weight, and the coronary arteries and fine blood vessels were visible.

Figure 9 shows angiograms of a dog heart specimen of 65 mm thickness using iodine spheres with an exposure time of 60 s. Although the image contrast decreased slightly with increasing thickness of the PMMA plate facing the X-ray

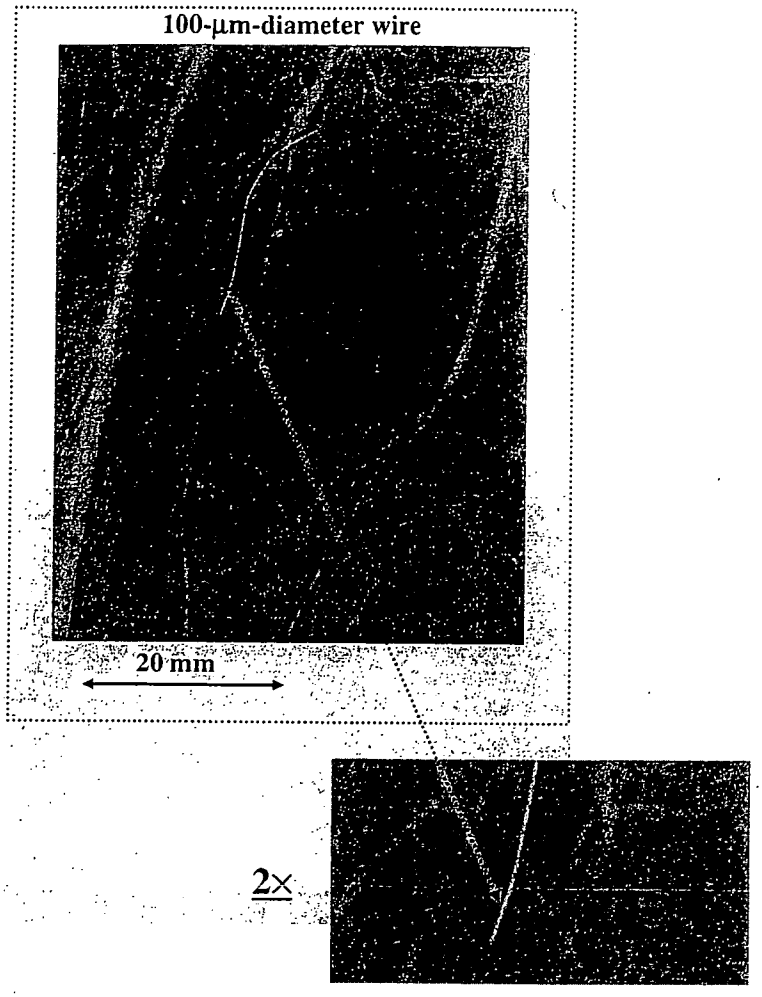

Fig. 8. Angiograms of rabbit thigh.

source, the coronary arteries of approximately 100 μm diameter were observed using a 100-mm-thick plate.

5. Conclusions

We employed a microfocus X-ray generator with a tungsten target tube to perform enhanced magnification angiography using narrow-photon-energy bremsstrahlung X-rays at a peak photon energy of approximately 38 keV, which can be absorbed easily by iodine-based contrast media. Although bremsstrahlung X-ray intensity substantially increased with increasing tube voltage, the optimal tube voltage for increasing image contrast was determined to be 60 kV.

Because the sampling pitch of the CR system is 87.5 μm, we obtained spatial resolutions of approximately 50 μm using fourfold magnification imaging achieved with a 20-μm-focus tube. To observe fine blood vessels of less than 100 μm diameter, the spatial resolution of the CR system should be improved to 43.8 μm (Regius 190, Konica Minolta), and iodine density should be increased.

In this research, we controlled bremsstrahlung X-rays to the optimum spectral distribution for realizing enhanced angiography using iodine-based contrast media. On the other hand, gadolinium-based contrast media with a K-edge energy of 50.2 keV have been employed to perform angiography in MRI, and the gadolinium density used has been increasing. In view of this situation, tungsten Kα rays (58.9 keV) are useful for enhancing K-edge angiography, because the Kα rays are absorbed effectively by gadolinium media. As compared with angiography using iodine media, the absorbed dose can be decreased considerably using gadolinium media.

At a tube voltage of 60 kV and a current of 170 μA, the photon number was approximately 2×10^7 photons/(cm^2·s) at 1.0 m from the source, and photon count rate can be increased easily using a rotating anode microfocus tube developed by Hitachi Medical Corporation. Recently, the maximum electric power of the microfocus X-ray tube has been increasing, and a kilowatt-range tube is realizable. Therefore, real-time magnification radiography will become possible using a flat panel detector with a pixel size of less than 100 μm.

Acknowledgments

This work was supported by Grants-in-Aid for Scientific Research (13470154, 13877114, and 16591222) and Advanced Medical Scientific Research from MECSST, Health and Labor Sciences Research Grants (RAMT-nano-001, RHGTEFB-genome-005 and RHGTEFB-saisei-003), and grants from the Keiryo Research Foundation, Promotion and Mutual Aid Corporation for Private Schools of Japan, Japan Science and Technology Agency (JST), and New Energy and Industrial Technology Development Organization (NEDO, Industrial Technology Research Grant Program in '03).

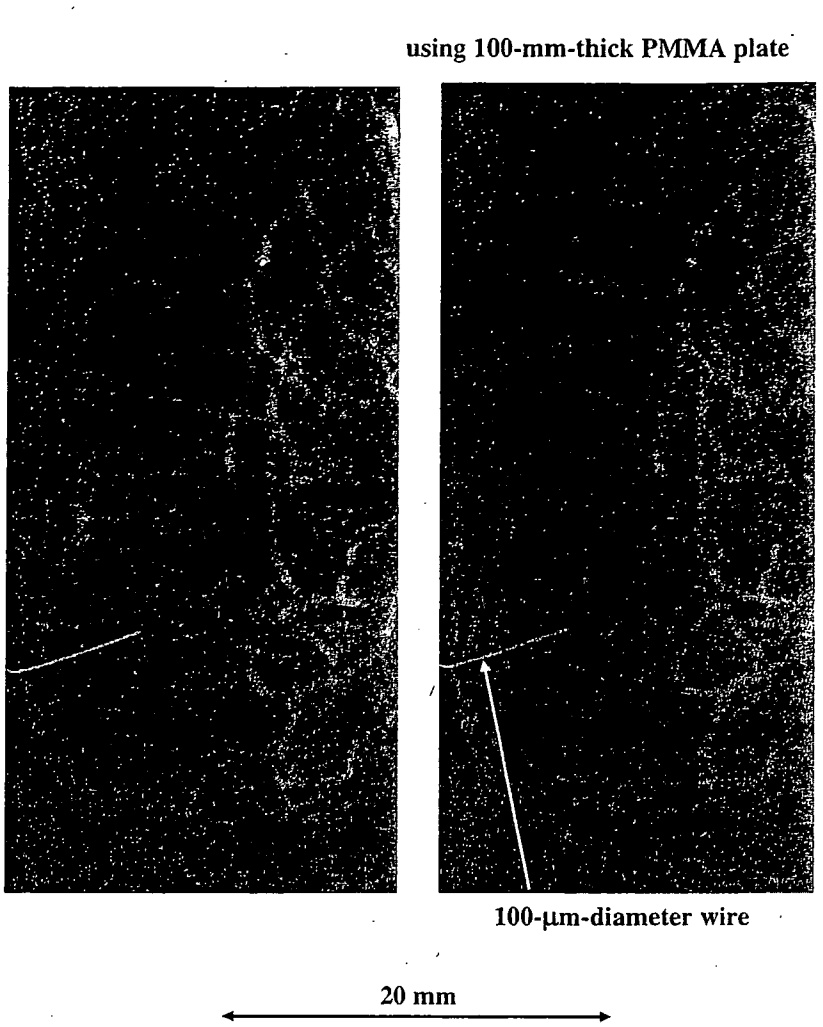

Fig. 9. Angiograms of extracted dog heart.

1) E. Sato, S. Kimura, S. Kawasaki, H. Isobe, K. Takahashi, Y. Tamakawa and T. Yanagisawa: Rev. Sci. Instrum. **61** (1990) 2343.
2) K. Takahashi, E. Sato, M. Sagae, T. Oizumi, Y. Tamakawa and T. Yanagisawa: Jpn. J. Appl. Phys. **33** (1994) 4146.
3) E. Sato, K. Takahashi, M. Sagae, S. Kimura, T. Oizumi, Y. Hayasi, Y. Tamakawa and T. Yanagisawa: Med. Biol. Eng. Comput. **32** (1994) 289.
4) E. Sato, M. Sagae, K. Takahashi, A. Shikoda, T. Oizumi, Y. Hayasi, Y. Tamakawa and T. Yanagisawa: Med. Biol. Eng. Comput. **32** (1994) 295.
5) E. Sato, Y. Hayasi, R. Germer, E. Tanaka, H. Mori, T. Kawai, T. Ichimaru, K. Takayama and H. Ido: Rev. Sci. Instrum. **74** (2003) 5236.
6) E. Sato, Y. Hayasi, R. Germer, E. Tanaka, H. Mori, T. Kawai, T. Ichimaru, S. Sato, K. Takayama and H. Ido: J. Electron Spectrosc. Relat. Phenom. **137–140** (2004) 713.
7) E. Sato, E. Tanaka, H. Mori, T. Kawai, S. Sato and K. Takayama: Opt. Eng. **44** (2005) 049002.
8) E. Sato, M. Sagae, E. Tanaka, Y. Hayasi, R. Germer, H. Mori, T. Kawai, T. Ichimaru, S. Sato, K. Takayama and H. Ido: Jpn. J. Appl. Phys. **43** (2004) 7324.
9) E. Sato, E. Tanaka, H. Mori, T. Kawai, T. Ichimaru, S. Sato, K. Takayama and H. Ido: Med. Phys. **32** (2005) 49.
10) E. Sato, Y. Hayasi, K. Kimura, E. Tanaka, H. Mori, T. Kawai, T. Inoue, A. Ogawa, S. Sato, K. Takayama, J. Onagawa and H. Ido: Jpn. J. Appl. Phys. **44** (2005) 8716.
11) A. Momose, T. Takeda, Y. Itai and K. Hirano: Nat. Med. **2** (1996) 473.
12) M. Ando, A. Maksimenko, H. Sugiyama, W. Pattanasiriwisawa, K. Hyodo and C. Uyama: Jpn. J. Appl. Phys. **41** (2002) L1016.
13) H. Mori, K. Hyodo, E. Tanaka, M. U. Mohammed, A. Yamakawa, Y. Shinozaki, H. Nakazawa, Y. Tanaka, T. Sekka, Y. Iwata, S. Honda, K. Umetani, H. Ueki, T. Yokoyama, K. Tanioka, M. Kubota, H. Hosaka, N. Ishizawa and M. Ando: Radiology **201** (1996) 173.
14) K. Hyodo, M. Ando, Y. Oku, S. Yamamoto, T. Takeda, Y. Itai, S. Ohtsuka, Y. Sugishita and J. Tada: J. Synchrotron Radiat. **5** (1998) 1123.
15) S. W. Wilkins, T. E. Gureyev, D. Gao, A. Pogany and A. W. Stevenson: Nature **384** (1996) 335.
16) A. Ishisaka, H. Ohara and C. Honda: Opt. Rev. **7** (2000) 566.
17) E. Sato, K. Sato and Y. Tamakawa: Annu. Rep. Iwate Med. Univ. School Liberal Arts Sci. **35** (2000) 13.
18) E. Sato, E. Tanaka, H. Mori, T. Kawai, T. Ichimaru, S. Sato, K. Takayama and H. Ido: Med. Phys. **31** (2004) 3017.
19) E. Sato, E. Tanaka, H. Mori, T. Kawai, T. Inoue, A. Ogawa, A. Yamadera, S. Sato, F. Ito, K. Takayama, J. Onagawa and H. Ido: Jpn. J. Appl. Phys. **44** (2005) 8204.
20) A. B. Crummy, C. A. Mistretta, M. G. Ort, F. Kelcz, J. R. Cameron and M. P. Siedband: Radiology **8** (1973) 402.
21) R. A. Kruger, C. A. Mistretta, A. B. Crummy, J. F. Sackett, M. M. Goodsit, S. J. Riederer, T. L. Houk, C. G. Shaw and D. Flemming: Radiology **125** (1977) 234.
22) F. Kelcz and C. A. Mistretta: Med. Phys. **3** (1977) 159.

Available online at www.sciencedirect.com

SCIENCE DIRECT

Life Sciences 78 (2006) 882 – 887

Life Sciences

www.elsevier.com/locate/lifescie

Vagal stimulation suppresses ischemia-induced myocardial interstitial norepinephrine release

Toru Kawada [a,*], Toji Yamazaki [b], Tsuyoshi Akiyama [b], Meihua Li [a], Hideto Ariumi [a], Hidezo Mori [b], Kenji Sunagawa [c], Masaru Sugimachi [a]

[a] *Department of Cardiovascular Dynamics, Advanced Medical Engineering Center, National Cardiovascular Center Research Institute, 5-7-1 Fujishirodai, Suita, Osaka 565-8565, Japan*

[b] *Department of Cardiac Physiology, National Cardiovascular Center Research Institute, Osaka 565-8565, Japan*

[c] *Department of Cardiovascular Medicine, Graduate School of Medical Sciences, Kyushu University, Fukuoka 812-8582, Japan*

Received 30 November 2004; accepted 31 May 2005

Abstract

Although electrical vagal stimulation exerts beneficial effects on the ischemic heart such as an antiarrhythmic effect, whether it modulates norepinephrine (NE) and acetylcholine (ACh) releases in the ischemic myocardium remains unknown. To clarify the neural modulation in the ischemic region during vagal stimulation, we examined ischemia-induced NE and ACh releases in anesthetized and vagotomized cats. In a control group (VX, $n=8$), occlusion of the left anterior descending coronary artery increased myocardial interstitial NE level from 0.46±0.09 to 83.2±17.6 nM at 30–45 min of ischemia (mean±SE). Vagal stimulation at 5 Hz (VS, $n=8$) decreased heart rate by approximately 80 beats/min during the ischemic period and suppressed the NE release to 24.4±10.6 nM ($P<0.05$ from the VX group). Fixed-rate ventricular pacing (VSP, $n=8$) abolished this vagally mediated suppression of ischemia-induced NE release. The vagal stimulation augmented ischemia-induced ACh release at 0–15 min of ischemia (VX: 11.1±2.1 vs. VS: 20.7±3.9 nM, $P<0.05$). In the VSP group, the ACh release was not augmented. In conclusion, vagal stimulation suppressed the ischemia-induced NE release and augmented the initial increase in the ACh level. These modulations of NE and ACh levels in the ischemic myocardium may contribute to the beneficial effects of vagal stimulation on the heart during acute myocardial ischemia.

Keywords: Acetylcholine; Coronary occlusion; Ventricular pacing

Introduction

Acute myocardial ischemia disrupts normal neural regulation of the heart (Armour, 1999). During prolonged ischemia, myocardial interstitial norepinephrine (NE) and acetylcholine (ACh) levels are increased in the ischemic region via local releasing mechanisms independent of efferent autonomic activities (Schömig et al., 1987; Lameris et al., 2000; Kawada et al., 2000, 2001). The excess NE release is thought to aggravate ischemic injury to the myocardium (Schömig et al., 1987). On the other hand, vagal stimulation exerts antiarrhythmic effects in the early phase of acute myocardial ischemia (Rosenshtraukh et al., 1994; Vanoli et al., 1991). A recent study from our laboratory demonstrated that vagal stimulation improved the survival rate of chronic heart failure after myocardial infarction in rats (Li et al., 2004), suggesting a long-term ameliorative effect of direct neural interventions against certain heart diseases.

With respect to electrical stimulation of the vagus, whether it alters myocardial interstitial NE and ACh levels in the ischemic region during acute myocardial ischemia remains unknown. To test the hypothesis that vagal stimulation increases the ACh level and suppresses the NE level in the ischemic region, we measured myocardial interstitial NE and ACh levels during acute myocardial ischemia in anesthetized cats using a cardiac microdialysis technique (Akiyama et al., 1991, 1994; Yamazaki et al., 1997). Effects of vagal stimulation were examined with or without fixed-rate ventricular pacing.

* Corresponding author. Tel.: +81 6 6833 5012x2427; fax: +81 6 6835 5403.
E-mail address: torukawa@res.ncvc.go.jp (T. Kawada).

0024-3205/$ - see front matter © 2005 Elsevier Inc. All rights reserved.
doi:10.1016/j.lfs.2005.05.087